# $MnO_2$ nanoparticles trigger hepatic lipotoxicity and mitophagy via mtROS-dependent $Hsf1^{Ser326}$ phosphorylation

Tao Zhao[a,1], Hua Zheng[a,1], Jie-Jie Xu[a], Kostas Pantopoulos[c], Yi-Chuang Xu[a], Lu-Lu Liu[a], Xi-Jun Lei[a], Yannis P. Kotzamanis[d], Zhi Luo[a,b,*]

[a] Hubei Hongshan Laboratory, Fishery College, Huazhong Agricultural University, Wuhan 430070, China

[b] Laboratory for Marine Fisheries Science and Food Production Processes, Qingdao National Laboratory for Marine Science and Technology, Qingdao 266237, China

[c] Lady Davis Institute for Medical Research and Department of Medicine, McGill University, Montreal, Quebec H3T 1E2, Canada

[d] Institute of Marine Biology, Biotechnology and Aquaculture, Hellenic Centre for Marine Research, Agios Kosmas, Hellenikon, 16777Athens, Greece

*Corresponding author. Prof. Zhi Luo, Tel.: +86-27-8728-2113; Fax: +86-27-8728-2114; Email address: luozhi99@mail.hzau.edu.cn; luozhi99@aliyun.com (Z. Luo).

[1]These authors contributed equally.

## Abstract

Manganese (Mn) is an essential element for maintaining normal metabolism in vertebrates. Mn dioxide nanoparticles ($MnO_2$ NPs), a novel Mn source, have shown great potentials in biological and biomedical applications due to their distinct physical and chemical properties. However, little is known about potential adverse effects on animal or cellular metabolism. Here, we investigated whether and how dietary $MnO_2$ NPs affect hepatic lipid metabolism in vertebrates. We found that, excessive $MnO_2$ NPs intake increased hepatic and mitochondrial Mn content, promoted hepatic lipotoxic disease and lipogenesis, and inhibited hepatic lipolysis and fatty acid β-oxidation. Moreover, excessive $MnO_2$ NPs intake induced hepatic mitochondrial oxidative stress, damaged mitochondrial function, disrupted mitochondrial dynamics and activated mitophagy. Importantly, we uncovered that mtROS-activated phosphorylation of heat

shock factor 1 (Hsf1) at Ser326 residue mediated $MnO_2$ NPs-induced hepatic lipotoxic disease and mitophagy. Mechanistically, $MnO_2$ NPs-induced lipotoxicity and mitophagy were via mtROS-induced phosphorylation and nucleus translocation of Hsf1 and its DNA binding capacity to *plin2*/*dgat1* and *bnip3* promoters, respectively. Overall, our findings uncover novel mechanisms by which mtROS-mediated mitochondrial dysfunction and phosphorylation of $Hsf1^{S326}$ contribute to $MnO_2$ NPs-induced hepatic lipotoxicity and mitophagy, which provide new insights into the effects of metal oxides nanoparticles on hepatotoxicity in vertebrates.

*Keywords:* Mn dioxide nanoparticles; Hepatotoxicity; Mitochondrial oxidative stress; Mitophagy; Lipotoxicity

## 1. Introduction

In recent years, nanoparticles have been largely produced and extensively applied in various fields, such as medicine, animal husbandry, battery technologies and sewage treatment, due to their unique physical properties at the nano scale [1-3]. Metal oxide nanoparticles are regarded as highly versatile materials among all the nanomaterials currently in use, owing to their diverse range of properties and functionalities. Particularly, Mn dioxide ($MnO_2$) nanoparticles (NPs) are among the metal oxide nanoparticles widely utilized in biosensors, biomedical devices, fertilizers, drug-delivery, contrast agents for magnetic resonance imaging, wastewater treatment and feed additives [1,4-6]. Global $MnO_2$ NPs production can reach up to 1000 tons per year and is considered to be “mass production” [7]. Significantly, along with the extensive application of $MnO_2$ NPs, their potential effects on animals and human health have attracted increasing attention. Among various exposure routes to NPs, dietary exposure is recognized as one of the most crucial in humans [8,9], and aquatic organisms [10]. Experimental data suggest that $MnO_2$ NPs induced neuronal oxidative stress in PC12 cells and rats [11,12]. Exposure to high-concentrations of $MnO_2$ NPs also induced abnormal neurobehavior, damaged memory function in rats, caused significant histological alterations and Mn accumulation in rats [13,14]. Additionally, $MnO_2$ nanosheets induced mitochondrial toxicity in fish gill epithelial cells [15]. However,

although many studies have shown that $MnO_2$ NPs cause harmful biological responses in various organisms, the underlying mechanisms are largely unclear.

The liver is the major solid organ for the NPs accumulation [16,17]. It is also the central organ for lipid metabolism, which is crucial to maintain physiological functions of the organisms [17,18]. There is increasing evidence that exposure to metal nanoparticles can cause lipid metabolism disorders such as non-alcoholic fatty liver disease (NAFLD), which is characterized by excessive accumulation of lipid droplets (LDs) in hepatocytes [17,19]. To date, only few studies have demonstrated $MnO_2$ NPs-induced liver damage in rats and mice [14,20]. However, the underlying mechanisms remain largely unexplored. Studies demonstrated that oxidative stress disrupts hepatic lipid metabolism and induces lipotoxic disease, thereby initiating the development of NAFLD [17,18,21,22]. Furthermore, oxidative stress has been identified as the primary factor contributing to the cytotoxicity induced by $MnO_2$ NPs [23,24]. Our recent publication pointed out that $MnO_2$ NPs promote lipid uptake and lipogenesis and trigger oxidative stress in the intestine of yellow catfish [25], but the effects and exact mechanism is unclear in the liver tissues. Importantly, HSF1 has been demonstrated to be a sensor of redox homeostasis [22,26,27]. Under oxidative stress, Hsf1 translocates to the nucleus and binds to conserved heat shock-responsive DNA elements (HSEs) to upregulate transcription of heat shock proteins (HSPs); these serve as molecular chaperones to protect cells from stress [26]. Hsf1 can also regulate lipid metabolism [22,28,29]. During cellular stress, Hsf1 undergoes phosphorylation at serine 326 (S326), which is a critical posttranslational modification (PTM) for its transcriptional activation [30]. However, it is still unclear whether these responses are related to the regulation of $MnO_2$ NPs-induced hepatic lipid metabolism.

At elevated concentrations, $MnO_2$ NPs exhibit cytotoxicity mainly due to their reactivity with biological systems and their enhanced potentials for cellular uptake [24]. Their main target are mitochondria, which are highly dynamic and multifunctional organelles that play a critical role in keeping cellular functions [23,31]. Several studies have indicated that $MnO_2$ NPs induce oxidative stress and damage the mitochondrial structure and function [15,23,24,31]. Mitochondrial balance is maintained by two

interconnected processes, mitochondrial dynamics and mitophagy [32]. The removal of damaged mitochondria, known as mitophagy, is an evolutionarily conserved process that plays a crucial role in maintaining cellular homeostasis [33]. Mitophagy is primarily governed by two molecular pathways: a) the PINK1 (PTEN induced kinase 1)/PRKN (parkin RBR E3 ubiquitin protein ligase)-dependent mitophagy mediated by the ubiquitin proteasome system [33], and b) mitophagy receptors-mediated mitophagy, such as BCL2 and adenovirus E1B 19-kDa-interacting protein 3 (Bnip3), BNIP3-like (Bnip3l), FUN14 domain-containing protein 1 (Fundc1), FK506-binding protein 8 (Fkbp8), and Bcl2-like 13 (Bcl2l13) [34]. Bnip3 is highly expressed in the liver and directly interacts with LC3B to initiate the process of mitophagy [34]. Several studies have indicated that Bnip3-mediated mitophagy contributes to protection against liver injury and relief of hepatic lipid deposits [35,36]. Excessive ROS generation by metals or metal nanoparticles exposure leads to mitochondrial dysfunction and activation of Bnip3-dependent mitophagy [37,38]. However, the effects and underlying mechanisms of $MnO_2$ NPs on mitophagy have not been elucidated.

Fish have almost 30,000 species and are the biggest group of vertebrates in the world. Their metabolic reaction pathways and nutrient-sensing systems are evolutionarily conserved with mammals [18,39]. Yellow catfish *Pelteobagrus fulvidraco*, a freshwater economic fish widely farmed in China and other countries [40], is an excellent model for studying lipid metabolism since it has a lipid metabolism pattern similar to that of mammals and its complete genome sequence were published and available internationally [39-41]. Moreover, many studies have used yellow catfish as a model to analyze the mechanism and treatment of metabolic disorders [18,41-44], and have attracted wide attention by international researchers [45,46, 47]. Therefore, *P. fulvidraco* provides an excellent experimental model to identify regulatory mechanisms of lipid metabolism. Therefore, the aim of this study was to explore the mechanisms of $MnO_2$ NPs-induced changes of lipid metabolism in the liver of yellow catfish. Our study reveals an unprecedented significant regulatory role of mtROS-triggered $Hsf1^{S326}$ phosphorylation in $MnO_2$ NPs-induced hepatic lipotoxicity and mitophagy. Importantly, we identified novel targets of Hsf1 mediating lipogenesis and

mitophagy, and correspondingly strengthened the role of Hsf1 as a regulator of hepatic lipid metabolism. Our findings provide new insights into the effects of metal oxides nanoparticles on hepatotoxicity in vertebrates.

## 2. Materials and methods

### *2.1. Ethical standards*

The experiments protocols for animal feeding and sampling, and cell culture followed the Huazhong Agricultural University (HZAU) ethical guidelines on the care and usage of laboratory animals and cells, and were authorized by the HZAU Ethic Committee.

### *2.2. $MnO_2$ NPs preparation*

A stock solution of 20 mg/ml $MnO_2$ NPs (≥99.5% in purity, 50 ± 10 nm, Xiya Chemical Technology Co. Ltd., Jinan, China) was prepared by dispersing the nanoparticles in deionized water. The physico-chemical characteristics of $MnO_2$ NPs were described in our recent study [48].

### *2.3. Diets preparation, animal feeding and sampling*

The approach to diet preparation was similar to that described in our recent study [49]. Three experimental diets were formulated with $MnO_2$ NPs (50 nm, ≥99.5% of the purity, Xiya Chemical Technology Co. Ltd., Shandong, China) levels of 0 (control), 20 mg/kg $MnO_2$ NPs (low $MnO_2$ NPs), 80 mg/kg $MnO_2$ NPs (high $MnO_2$ NPs) (Supplementary Table 1). Final Mn contents in diets were measured using ICP-OES (Optima 8000DV; PerkinElmer, MA, USA), and the contents were 1.67, 13.63, and 50.37 mg/kg for the control, low $MnO_2$ NPs, and high $MnO_2$ NPs groups, respectively. Based on Xu et al. [49], dietary Mn requirement was 8.33-12.57 mg/kg diet for *P. fulvidraco* with $MnO_2$ NPs as Mn source.

The animal feeding protocols were described in our recent study [25, 49]. Briefly, a total of 225 uniformly sized yellow catfish (2.82 ± 0.01 g, mean ± SEM) were equally assigned to nine tanks (300 L water volume), 25 fish each tank, and three replicate tanks per treatment. Fish were fed to satiation twice daily (08:30 and 16:30) for 8 weeks. During the experiment, the concentration of Mn in rearing water was detected twice per

week using the ICP-OES and the values were below detection limit (<1 μg/L).

Sampling was conducted after the 8-wk feeding experiment, and the detailed sampling methods are presented in Text S1.

*2.4. Yellow catfish hepatocytes isolation, culture and treatments*

The protocols for isolation and culture of yellow catfish hepatocytes were described in our recent studies [22,43]. The treatment concentrations and time for all *in vitro* experiments are presented in the figure legends.

*2.5. Serum biochemical analysis*

Serum aspartate aminotransferase (AST) and alanine aminotransferase (ALT) activities were determined by commercial kits (C010-2-1 and C009-2-1, Nanjing Jiancheng Bioengineering Institute, Nanjing, China).

*2.6. Histological, histochemical and ultrastructural observation*

The liver tissues were stained with hematoxylin−eosin (H&E) (G1120; Solarbio, Beijing, China) and oil red O (ORO) (G1260; Solarbio) for vacuoles and lipid droplets observation, respectively, and yellow catfish hepatocytes were stained with BODIPY493/503 (D3922; Thermo Fisher Scientific) for lipid droplets visualization, as described in our recent publications [17,22]. Ten areas were randomly examined from each sample to analyze the relative areas of liver vacuoles with the H&E staining and lipid droplets with the ORO staining, and quantified by using the Image J software. The BODIPY493/503 fluorescent intensity was quantified by CytoFLEX flow cytometry (Beckman Coulter, Miami, USA). The lipid droplet images were acquired by the instrument TCS SP8 LSCM (laser scanning confocal microscope) (Leica, Wetzlar, Germany). The experimental protocols for ultrastructural observation were described in our recent publications [17,22].

*2.7. Liver mitochondrial isolation*

Mitochondria were isolated from fresh livers as previously reported [41,48]. The purified mitochondria were used to analyze protein expression and Mn content.

*2.8. Analysis of cell viability, non-esterified free fatty acids (NEFAs), triglycerides (TGs) and Mn content*

CCK-8 kit (C0037, Beyotime, Beijing, China) was used to evaluate the cell

viability as reported by Zhao et al. [22]. The NEFAs, TG and protein concentration were measured using the commercial kits (A042-1-1, A110-1-1 and A045-2-2, Nanjing Jiancheng Corp., Nanjing, China). Mn contents in the experimental diets, liver tissues and isolated mitochondria were measured by the instrument ICP-OES (Optima 8000, PerkinElmer, Waltham, MA, USA) according to previous publications [25,48].

*2.9. Lactate dehydrogenase leakage assay*

LDH leakage in the medium was determined using the LDH assay kit (C0016, Beyotime) based on the manufacturer's instructions.

*2.10. Analysis of lipolytic enzyme activity and oxidative stress indicators*

The activity of lipolytic enzyme Cpt1 was measured based upon Zhao et al. [22]. Several markers of oxidative stress, such as, Sod2 and Cat activity, MDA and ATP content, the ratio of GSH/GSSG, mitochondria-derived $O_2^{\bullet-}$ content, and mitochondrial membrane potential (MMP) were determined, and the detailed methods are presented in Text S2.

*2.11. Quantification of mitochondrial DNA (mtDNA) copy number*

mtDNA copy number was quantified by real time quantitative PCR (qPCR) as reported previously [50]. Briefly, DNA was extracted from liver and hepatocytes by Tissue DNA Kit (D3396, OMEGA Bio-tek, Norcross, GA, USA), and qPCR for *atp8* and *eef1a* representing mitochondrial and nuclear DNA genes was conducted. The mtDNA level was calculated relative to nuclear DNA. The mtDNA primers are listed in Supplementary Table 2.

*2.12. RNA extraction and qPCR analysis*

RNA isolation and qPCR analysis were carried out according to protocols in [22,25], which are provided in Text S3. The gene-specific primers are presented in Supplementary Table 2.

*2.13. RNA interference*

The yellow catfish *hsf1* small interfering RNA (siRNA) and negative control (NC) were obtained from GenePharma (Shanghai, China). The procedure for siRNA transfection into primary hepatocytes is given in details in Text S4. The sequences of siRNA are provided in Supplementary Table 2.

*2.14. Plasmid construction and transient transfection*

The HEK 293T cells were used to explore effect of Hsf1 on transcriptional activity of downstream promoters. The expression plasmid for pcDNA3.1-HA-Hsf1 was constructed and transfected based on our methods [22,29], which are presented in Text S5. The primer sequences are given in Supplementary Table 2.

*2.15. Western blotting*

Western blotting was used to determine the expression levels of several proteins, such as Pparg, Dgat1, Plin2, p-Hsf1$^{S326}$, Hsf1, Mfn2, Drp1, Atg7, P62, Lc3b, Parkin, Bnip3, and Tom20 as described in previous studies [18,29]. The detailed methods are presented in Text S6.

*2.16. Immunofluorescence*

Immunofluorescence was performed according to previous publications [18,37], and detailed methods are provided in Text S7.

*2.17. Dual-luciferase reporter test*

Luciferase activity tests were performed according to our studies [18,22], and the details can be found in Text S8.

*2.18. Electrophoretic mobility shift assay (EMSA)*

EMSA was used to investigate the direct binding site of Hsf1 in the *bnip3*, *plin2* and *dgat1* promoters according to the protocols in our studies [22,29]. The detailed protocols are presented in Text S9. All the oligonucleotide sequences are given in Supplementary Table 2.

*2.19. Chromatin immunoprecipitation (ChIP) assay*

ChIP assay was carried out according to previously described methods [43,51], and the detailed methods are provided in Text S10. All primers used for ChIP-qPCR are shown in Supplementary Table 2.

*2.20. Statistical analysis*

The software SPSS 19.0 was used for the statistical analysis. All these data are presented as means ± SEM. Before statistical analysis, all the data were assessed for normality using a Kolmogorov–Smirnov test, and Bartlett's test was used to examine the homogeneity of the variances. One-way ANOVA and post hoc Duncan's multiple

range test were conducted to examine the statistical significance among the three groups. Student's *t*-test (unpaired, two-tailed) was used to analyze the difference between two treatments. Difference was thought significant when $P < 0.05$.

## 3. Results

### *3.1. In vivo study*

#### *3.1.1. $MnO_2$ NPs increase Mn content and affect Mn metabolism in the liver*

The Mn content of liver and hepatic mitochondria increased with dietary $MnO_2$ NPs levels (Supplementary Fig. 1A and B). Compared with the control and low $MnO_2$ NPs groups, high $MnO_2$ NPs increased the *dmt1*, *fpn1* and *zip8* mRNA expression, which encode metal transporters (Supplementary Fig. 1C). Dietary $MnO_2$ NPs reduced the *zip14* and *cav1* mRNA levels (Supplementary Fig. 1C and D). Besides, compared with control, high $MnO_2$ NPs upregulated mRNA levels of endocytosis-related genes (*dnm1* and *cltc*) and downregulated mRNA abundances of *dnm3* (Supplementary Fig. 1D).

#### *3.1.2 Effects of dietary $MnO_2$ NPs levels on the liver health of yellow catfish*

High dietary $MnO_2$ NPs significantly increased the serum AST and AST activities (Supplementary Fig. 2A and B), up-regulated the mRNA levels of inflammation-related genes (*il1β* and *tnfa*) and down-regulated the mRNA expression of *il10* (Supplementary Fig. 2C), but did not affect the *il6* and *il8* mRNA levels (Supplementary Fig. 2C), compared to other two groups. Additionally, high dietary $MnO_2$ NPs significantly increased the mRNA level of apoptosis-related genes (*bax*, *casp3*, and *cycs*) and decreased mRNA level of *bcl2* (Supplementary Fig. 2D). Overall, these results suggest that high dietary $MnO_2$ NPs damaged liver health of yellow catfish.

#### *3.1.3. $MnO_2$ NPs increase hepatic lipid content and lipogenesis, but reduce lipolysis and fatty acid oxidation*

The liver was enlarged and seemed white in yellow catfish fed with high $MnO_2$ NPs (Fig. 1A). Hepatic H&E and ORO staining showed that the amount of cytoplasmic vacuolation and lipid droplets increased with dietary $MnO_2$ NPs addition (Fig. 1B and C). In line with these data, the hepatic TGs content in the high $MnO_2$ group was also

higher than those in the other two groups (Fig. 1D). The quantification of cytoplasmic vacuolations and lipid droplets further confirmed these results (Fig. 1E and F).

Compared with the control and low $MnO_2$ NPs groups, high dietary $MnO_2$ NPs up-regulated the *6pgd*, *fas*, *plin2* and *dgat1* mRNA (lipogenic genes) and down-regulated mRNA expression of *cpt1* and *atgl* (lipolytic genes) (Supplementary Fig. 3A). Compared with the control, high dietary $MnO_2$ NPs significantly increased the *acca*, *srebp1c* and *pparg* mRNA levels (Supplementary Fig. 3A). Cpt1 activity was significantly lower for fish fed high $MnO_2$ NPs than those in the control and low $MnO_2$ NPs groups (Supplementary Fig. 3B). Additionally, high dietary $MnO_2$ NPs increased the protein levels of Pparg and Dgat1 (Supplementary Fig. 3C and D). The Plin2 protein levels in the high $MnO_2$ NPs group were higher compared to the control but did not differ from the low $MnO_2$ NPs group (Supplementary Fig. 3C and D). Additionally, high dietary $MnO_2$ NPs markedly down-regulated the expression of fatty acid oxidation-related genes (*acad8*, *acads*, *echs1*, and *eci*), but did not affect abundance of *acadl*, *acadsb*, and *hadha1* mRNAs (Supplementary Fig. 3E).

*3.1.4. $MnO_2$ NPs induce mitochondrial dysregulation and oxidative stress, increase $Hsf1^{S326}$ phosphorylation and promote Hsf1 nuclear translocation in the liver*

Some studies have shown that NPs-induced lipid metabolism disorders are related to mitochondrial dysfunction [10,17]. Next, we investigated the effects of dietary $MnO_2$ NPs on hepatic mitochondrial function and antioxidant capacity of yellow catfish. High dietary $MnO_2$ NPs significantly decreased hepatic mtDNA copy number and ATP content compared to the control and low $MnO_2$ NPs groups (Fig. 2A-C). Sod2 activity was the highest in the low $MnO_2$ NPs group and lowest in the high $MnO_2$ NPs group (Fig. 2D). The Cat activity decreased, while MDA content increased remarkably in the high $MnO_2$ NPs group compared to the other two groups (Fig. 2E and F). Moreover, the GSH to GSSG ratio declined with increasing $MnO_2$ NPs levels (Fig. 2G). High $MnO_2$ NPs decreased the mRNA abundance of antioxidant related genes (*sod2*, *cat*, *gpx4*, *nrf2*) and augmented the *keap1* mRNA levels (Fig. 2H). The HSPs serve as crucial effectors of defensive responses against oxidative stress [26]. Compared to the control, high $MnO_2$ NPs up-regulated the mRNA expression of *hspbp1*, *hsp90a* and *hsf1* (Fig.

2H).

Dayalan Naidu et al. suggested that the phosphorylation of $HSF1^{S303/307}$ inhibits Hsf1 transcriptional activity while phosphorylation of $Hsf1^{S326}$ contributes to Hsf1 activation [52]. Therefore, the phosphorylation of $Hsf1^{S326}$ was investigated. Compared with control and $MnO_2$ NPs groups, high $MnO_2$ NPs increased the protein abundance of p-$Hsf1^{S326}$ and N-Hsf1 (Fig. 2I and J). Furthermore, high $MnO_2$ NPs increased total Hsf1 protein levels (Fig. 2I and J). Immunofluorescence analysis confirmed that $MnO_2$ NPs intake increased the expression and abundance of Hsf1 and promoted its nuclear translocation (Fig. 2K and L). Overall, these results indicated that $MnO_2$ NPs induced oxidative stress, increased $Hsf1^{S326}$ phosphorylation and promoted nuclear translocation of Hsf1.

*3.1.5. $MnO_2$ NPs exacerbate hepatic mitochondrial fission and inhibit mitochondrial fusion*

Mitochondrial fusion and fission are crucial for maintaining mitochondrial function [53]. Next, the mitochondrial dynamics-related genes and proteins expression were determined. Compared with control and low $MnO_2$ NPs groups, high $MnO_2$ NPs increased the mRNA levels of *drp1* and *fis1* (mitochondrial fission-related genes), and reduced the expression of *pgc1a* (mitochondrial biogenesis-related transcription factor) (Supplementary Fig. 4A), and *mfn2* (mitochondrial fusion-related gene) (Supplementary Fig. 4A). In addition, high dietary $MnO_2$ NPs increased the Drp1 and reduced the Mfn2 protein levels (Supplementary Fig. 4B and C). These results indicated that high dietary $MnO_2$ NPs exacerbate hepatic mitochondrial fission and inhibit mitochondrial fusion.

*3.1.6. $MnO_2$ NPs activate hepatic mitophagy*

Mitophagy is an important mitochondrial quality control mechanism that removes damaged mitochondria [17,32,33]. Therefore, we further explored the effects of dietary $MnO_2$ NPs on the process of mitophagy in the liver of yellow catfish. TEM images showed that dietary $MnO_2$ NPs addition increased the swelling and vesiculation of the mitochondria (Fig. 3A). The mRNA expression of mitophagy receptors-related genes (*bnip3*, *bnip3la*, and *march5*) and autophagy related genes (*ulk1*, *beclin1*, *ctsb*, and *tfeb)*

were remarkably induced in the high $MnO_2$ NPs group (Fig. 3B), but the mRNA levels of *parkin* and *pink1* (ubiquitin-mediated mitophagy-related genes) were not significantly affected. The Atg7 and Bnip3 protein abundances were notably higher, and P62 protein levels were lower in the high $MnO_2$ NPs group than those in other two groups (Fig. 3C and D). The Lc3bII protein levels were markedly higher, and the Tom20 protein levels lower in the high $MnO_2$ NPs group (Fig. 3C and D). In addition, high $MnO_2$ NPs notably increased Lc3bII and Bnip3 protein levels in the mitochondrial fraction compared to control (Fig. 3C and E). Immunofluorescence results revealed that high $MnO_2$ NPs increased the Bnip3 fluorescence intensity and the co-localization of Lc3 and Tom20, Bnip3 and Lc3 (Supplementary Fig. 5A-F). Overall, these results suggest that dietary $MnO_2$ NPs activate hepatic mitophagy.

### *3.2. In vitro Study*

#### *3.2.1. $MnO_2$ NPs increase TGs content in hepatocytes*

To further elucidate the mechanisms of $MnO_2$ NPs-induced lipotoxicity and mitophagy, several *in vitro* experiments were performed on yellow catfish hepatocytes. CCK8 assay showed that administration of 0–20 μg/ml of $MnO_2$ NPs did not remarkably affect the viability of yellow catfish hepatocytes (Supplementary Fig. 6A). The $IC_{50}$ of $MnO_2$ NPs on primary hepatocytes was 44.45 μg/ml (Supplementary Fig. 6B). Meanwhile, 0-20 μg/ml $MnO_2$ NPs increased TGs content in a concentration-dependent manner (Supplementary Fig. 6C), as also confirmed by BODIPY493/503 staining analysis (Supplementary Fig. 6D-F). Therefore, we chose 20 μg/ml $MnO_2$ NPs as the dose for our *in vitro* experiments.

#### *3.2.2. $MnO_2$ NPs trigger Pink1/parkin-independent mitophagy in hepatocytes*

Next, we investigated the effect of $MnO_2$ NPs on mitophagy in yellow catfish hepatocytes. The results showed that 20 μg/ml $MnO_2$ NPs obviously upregulated the *bnip3*, *ulk1*, *lc3b* and *tfeb* mRNA levels compared with the control and 10 μg/ml $MnO_2$ NPs groups (Fig. 4A), but there was no notable difference in the mRNA levels of *parkin*, *pink1*, *bnip3la*, *fundc1*, and *beclin1* among the three groups (Fig. 4A). The Bnip3 and Lc3bII protein levels were higher, and the protein levels of Tom20 and P62 were lower in the 20 μg/ml $MnO_2$ NPs versus the other groups (Fig. 4B and C). TEM analysis of

hepatocytes showed that a dose of 20 μg/ml $MnO_2$ NPs obviously increased the size and number of lipid droplets, and also the vacuoles enclosing mitochondria (red arrow) (Fig. 4D). Importantly, $MnO_2$ NPs were absorbed through endocytosis (yellow arrow) and deposited in the mitochondria (blue arrow) of hepatocytes (Fig. 4D). Immunofluorescence results showed that $MnO_2$ NPs significantly increased the colocalization of Bnip3 and Lc3, and Tom20 and Lc3 (Fig. 4E and F). Taken together, in agreement with our *in vivo* study, the $MnO_2$ NPs treatment activated Pink1/Parkin-independent mitophagy in primary hepatocytes.

*3.2.3. Mitochondrial ROS (mtROS) mediates $MnO_2$ NPs-induced mitochondrial dysfunction and lipotoxicity in hepatocytes*

To demonstrate the correlation between mitochondrial oxidative stress and lipotoxicity induced by $MnO_2$ NPs, Mito-TEMPO was used to eliminate mitochondrial ROS. Mito-TEMPO pre-incubation alleviated $MnO_2$ NPs-induced cytotoxicity and LDH leakage (Supplementary Fig. 7A and B). Mito-TEMPO pre-incubation mitigated the $MnO_2$ NPs-induced increase in mitochondrial $O_2^{\bullet-}$ content as confirmed by MitoSOX staining (Supplementary Fig. 8A, B and 9A). Mito-TEMPO treatment also revoked the $MnO_2$ NPs-induced reduction in Cat and Sod2 activities, ATP content, and mitigated $MnO_2$ NPs-induced increase of MDA content (Supplementary Fig. 8C-F). Moreover, Mito-TEMPO pretreatment alleviated $MnO_2$ NPs-induced decrease in mtDNA copy number (Supplementary Fig. 8G and H). $MnO_2$ NPs increased NEFA content, and this effect was reversed by Mito-TEMPO pre-incubation (Supplementary Fig. 8I). JC-1 and MitoTracker Deep Red staining revealed that $MnO_2$ NPs incubation reduced mitochondrial membrane potential (MMP), while Mito-TEMPO pre-treatment obviously abolished these effects (Supplementary Fig. 8J, K, L and 9B). In addition, Mito-TEMPO pretreatment remarkably alleviated $MnO_2$ NPs-induced increase in TGs content and the fluorescence intensity of BODIPY493/503 (Supplementary Fig. 10A-D), and relieved the Mn-induced reduction in Cpt 1 activity (Supplementary Fig. 10E). Furthermore, $MnO_2$ NPs incubation up-regulated the expression of lipogenic genes (*fas*, *acca*, *plin2*, *dgat1*, *pparg*, and *srebp1c*), and down-regulated the expression of lipolytic genes (*cpt1* and *ppara*), while these effects were abolished by Mito-TEMPO

pretreatment (Supplementary Fig. 10F). Overall, these findings suggest that mtROS mediated $MnO_2$ NPs-induced mitochondrial dysfunction and lipotoxicity in the primary hepatocytes of yellow catfish.

*3.2.4. Mito-TEMPO incubation inhibits $MnO_2$ NPs-activated mitophagy in hepatocytes*

We subsequently examined whether mitochondrial oxidative stress contributes to $MnO_2$ NPs-induced mitophagy in hepatocytes. The mRNA expressions of *bnip3*, *atg7*, *lc3b* and *tfeb* were significantly up-regulated by $MnO_2$ NPs treatment, while Mito-TEMPO pre-incubation abolished these changes (Supplementary Fig. 11A). Mito-TEMPO pre-incubation markedly blunted $MnO_2$ NPs-induced increase in protein levels of Bnip3 and Lc3bII, and the decrease in protein level of Tom20 and P62 (Supplementary Fig. 11B and C). Immunofluorescence demonstrated that the colocalization of Lc3 and Bnip3 was apparently increased by $MnO_2$ NPs, while Mito-TEMPO pre-incubation attenuated this effect (Supplementary Fig. 11D and E). These results suggest an involvement of mtROS in $MnO_2$ NPs-induced mitophagy.

*3.2.5. Mitochondrial oxidative stress is involved in $MnO_2$ NPs-induced phosphorylation at S326 and nuclear translocation of Hsf1 in hepatocytes*

Our *in vivo* study showed that $MnO_2$ NPs triggered phosphorylation of Hsf1 at S326 and promoted its nuclear translocation. Meanwhile, our previous study also suggested that Mn overload-induced oxidative stress contributes to induction of Hsf1 expression [22]. Thus, we further investigated whether the mtROS was directly involved in $Hsf1^{S326}$ phosphorylation and nuclear translocation. Mito-TEMPO alleviated $MnO_2$ NPs-induced increase in the mRNA expression of *hsf1*, and the protein levels of p-$Hsf1^{S326}$ and nuclear Hsf1 (Supplementary Fig. 12A and B). Immunofluorescence confirmed that $MnO_2$ NPs increased Hsf1 abundance, and promoted Hsf1 nuclear translocation, while these responses were attenuated by Mito-TEMPO pre-treatment (Supplementary Fig. 12C). To further elucidate the roles of $MnO_2$ NPs themselves and $Mn^{2+}$ released from $MnO_2$ NPs on Hsf1 nuclear translocation, we determined the concentration of $Mn^{2+}$ dissociated from $MnO_2$ NPs, as shown in Supplementary Table 3. Then, the $MnO_2$ NPs and $MnCl_2$ were used to incubate hepatocytes. Compared with the control, $MnO_2$ NPs increased the expression of N-Hsf1, while $MnCl_2$ had no effect

on the expression of N-Hsf1 (Supplementary Fig. 13A and B). Furthermore, immunofluorescence also confirmed these results (Supplementary Fig. 13C). Thus, $MnO_2$ NPs-induced nuclear translocation of Hsf1 depend on the properties of $MnO_2$ NPs themselves. *3.2.6. Hsf1 mediates $MnO_2$ NPs-induced mitophagy through transcriptional activation of bnip3 in hepatocytes*

Previous studies pointed out that, phosphorylation of Hsf1 at S326 strongly activates its transcriptional activity by promoting Hsf1 translocation into the nucleus for binding to conserved HSEs of its target gene promoters [54-56]. Thus, we explored the role of Hsf1 in regulating $MnO_2$ NPs-induced mitophagy by using the small interference RNA si-*hsf1*. Pretreatment with the *si-hsf1* eliminated the $MnO_2$ NPs-induced elevation in mRNA expression of *bnip3*, *atg7*, *lc3b*, and *tfeb* (Fig. 5A), and the protein levels of Bnip3 and Lc3b, and reversed the $MnO_2$ NPs-induced decrease in Tom20 and P62 protein abundance (Fig. 5B and C). Besides, *si-hsf1* pre-incubation also abolished the increase in co-localization of Lc3 and Bnip3 induced by $MnO_2$ NPs (Fig. 5D and E). These data suggest that activation of Hsf1 is essential for $MnO_2$ NPs-induced mitophagy.

We then explored the mechanism of Hsf1 mediating $MnO_2$ NPs-induced mitophagy by analyzing the promoter of the mitophagy-related gene *bnip3*. We identified a conservative HSE sequence (-nGAAn–) on the *bnip3* promoter in yellow catfish, which was positioned between -922 and -893 bp (Fig. 6A). $MnO_2$ NPs incubation significantly increased reporter luciferase activity of the *bnip3* promoter, and this effect was abolished by HSE mutation (Fig. 6B). Meanwhile, Hsf1 overexpression increased luciferase activity of the *bnip3* promoter, and this effect was reversed by HSE mutation (Fig. 6C and D). EMSA and chIP were performed to investigate whether Hsf1 can directly bind to the *bnip3* promoter (Fig. 6E-G). Remarkably, EMSA showed that the HSE sequences of the *bnip3* promoter could bind to the nuclear extract, and the interaction was hindered by unlabeled competitor wild type but not mutant probes (Fig. 6E). Besides, the binding activity of HSE to the nuclear extract was enhanced upon $MnO_2$ NPs incubation (Fig. 6E, lane 5). Importantly, a ChIP assay also confirmed that Hsf1 interacted with the *bnip3* promoter, and $MnO_2$ NPs treatment increased the Hsf1

452 binding (Fig. 6F and G). Thus, we demonstrate that Hsf1 mediates $MnO_2$ NPs-induced
453 mitophagy through transcriptional activation of *bnip3* in hepatocytes.
454 *3.2.7. Hsf1 mediates $MnO_2$ NPs-induced lipotoxicity through transcriptional activation*
455 *of plin2 and dgat1 in hepatocytes*
456 Next, we investigated the role of oxidative stress-mediated Hsf1 activation in
457 regulating $MnO_2$ NPs-induced lipotoxicity. We found that si-*hsf1* alleviated the $MnO_2$
458 NPs-induced increase in TGs content and the BODIPY493/503 fluorescence intensity
459 (Fig. 7A-D). Moreover, si-*hsf1* pretreatment down-regulated the $MnO_2$ NPs-induced
460 elevation of the mRNA and protein levels of Dgat1 and Plin2 (Fig. 7E-G). We then
461 attempted to clarify the mechanism by which Hsf1 mediates $MnO_2$ NPs-induced
462 lipotoxicity through HSE. By analyzing the promoters of *plin2* and *dgat1* in yellow
463 catfish, we found that HSE sites were located at -755 to -725 bp of *plin2* and -868 to -
464 838 bp and -1391 to -1361 bp sites of *dgat1* promoter (Fig. 8A and B). Furthermore,
465 $MnO_2$ NPs treatment significantly enhanced the luciferase activities of *plin2* and *dgat1*
466 promoters, and these observations were reversed by HSE mutation on *plin2* and HSE
467 mutation site1 on *dgat1* (Fig. 8C and D). Meanwhile, Hsf1 overexpression also
468 increased the luciferase activities of *plin2* and *dgat1* promoters, and these changes were
469 abolished by HSE mutation on *plin2* and HSE mutation site1 on *dgat1* (Fig. 8E and F).
470 EMSA indicated that the putative HSE sequences of the *plin2* and *dgat1* promoters
471 could bind to the nuclear extract, and the interaction was disrupted by unlabeled wild
472 type but not mutant probes (Fig. 8G and H). Thus, the -755 to -725 bp site of *plin2* and
473 -868 to -838 bp site of *dgat1* promoter region could directly interact with Hsf1.
474 Importantly, the binding activity of HSE to nuclear extracts was enhanced upon $MnO_2$
475 NPs incubation (Fig. 8G and H, lane 5). A ChIP experiment also confirmed that Hsf1
476 could bind to the -755 to -725 bp site of *plin2* and -868 to -838 bp site of *dgat1*
477 promoters, and $MnO_2$ NPs treatment enhanced the binding activity of Hsf1 (Fig. 8I-K).
478 Overall, these findings reveal that Hsf1 promotes $MnO_2$ NPs-induced lipotoxicity
479 through transcriptional activation of *plin2* and *dgat1*.
480
481 **4. Discussion**

Despite the wide use of $MnO_2$ NPs in biology and biomedicine, little is known about whether and how they affected animal or cellular metabolism after long-term exposure. Here, we investigated the potential mechanisms by which dietary $MnO_2$ NPs affect hepatic lipid metabolism. Our main innovative findings are: (1) high dietary $MnO_2$ NPs increase hepatic and mitochondrial Mn levels, hepatic lipid content and lipogenesis, and concomitantly decrease hepatic lipolysis and fatty acid β-oxidation; (2) excessive $MnO_2$ NPs intake induces hepatic mitochondrial oxidative stress, disrupts mitochondrial dynamics and activates mitophagy; (3) mtROS-promoted $Hsf1^{S326}$ phosphorylation mediated $MnO_2$ NPs-induced hepatic lipotoxicity and mitophagy; (4) $MnO_2$ NPs-induced lipotoxicity involves mtROS-induced $Hsf1^{S326}$ phosphorylation and Hsf1 nuclear translocation for enhanced DNA binding to the *plin2*/*dgat1* promoters; (5) $MnO_2$ NPs-induced mitophagy occurs via mtROS-induced $Hsf1^{S326}$ phosphorylation and Hsf1 nuclear translocation and enhanced DNA binding to the *bnip3* promoter. Overall, for the first time, these findings reveal novel mechanism by which mtROS-mediated mitochondrial dysfunction and $Hsf1^{S326}$ phosphorylation contribute to $MnO_2$ NPs-induced hepatic lipotoxic disease and mitophagy. Our data provide new insights into the effects of metal oxides nanoparticles on physiological responses and metabolism in vertebrates.

The liver is the main site for Mn accumulation and metabolism. Our study validates that dietary intake of $MnO_2$ NPs increase hepatic Mn content, as reported by others [14]. Previous work showed that metal oxide nanoparticles are absorbed via dissolved ions and endocytosis routes in vertebrates [17,25]. Hepatic Mn metabolism is modulated by metal transporters (importers and exporters) [57,58]. Zip8 is located on the apical membrane of hepatocytes and is necessary for maintaining liver Mn homeostasis [59]. Zip14 is expressed at high levels in the liver and can import Mn [60]. Divalent metal transporter 1 (Dmt1) is the plasma membrane protein and the primary $Mn^{2+}$ importer for cellular Mn uptake [61]. Ferroportin 1 (Fpn1) is involved in the regulation of Mn efflux [62]. Studies showed that *ZIP8* mRNA expression was notably induced by Mn overload in HeLa cells [63]. Exposure to high Mn decreased Zip14 levels which help maintain their integrity by reducing Mn uptake [64]. We recently

reported that dietary $MnO_2$ NPs increase the *zip8* and *dmt1* mRNA expression in the yellow catfish intestine [25]. In the present study, the higher expression of endocytosis-relevant genes (*dnm*, *cltc* and *eps15*) in the high $MnO_2$ NPs group indicates that $MnO_2$ NPs are also internalized via endocytosis, as shown in other studies [10,65]. Thus, high dietary $MnO_2$ NPs increase hepatic Mn uptake and accumulation partially via endocytosis of nanoparticles.

The liver also performs crucial functions in metabolism and detoxification, which is affected by toxicant exposure [17,22]. Several studies have reported hepatotoxicity induced by exposure to metal oxide nanoparticles [17,66]. Serum AST and ALT activities, hepatic inflammation and apoptosis are the key indicators for assessing hepatotoxicity [19,39,67]. Several studies have indicated that $MnO_2$ NPs exposure increased serum AST activity in mice and rats [14,20]. Our study revealed that high dietary $MnO_2$ NPs significantly increased the activities of serum AST and ALT, suggesting excessive $MnO_2$ NPs caused liver injury in yellow catfish.

Inflammation responses are regulated by both pro-inflammatory (Il6, Il8, Il1β and Tnfα) and anti-inflammatory factors Il10 [25,39]. Our recent study indicated that $MnO_2$ NPs induced inflammation responses in liver of yellow catfish compared to $MnSO_4$ [68]. Here, we found that high dietary $MnO_2$ NPs significantly increased the mRNA expression of pro-inflammatory factors (*il1β* and *tnfa*) and decreased mRNA expression of anti-inflammatory factor (*il10*), suggesting that $MnO_2$ NPs promoted hepatic inflammation.

Hepatic apoptosis is also regarded as a prominent pathological characteristic in the majority of liver injury [69]. In present study, high dietary $MnO_2$ NPs increased the mRNA expressions of pro-apoptotic genes *bax*, *casp3* and *cycs* and decreased anti-apoptotic gene *bcl-2*. Other study also reported $MnO_2$ NPs exposure induced apoptosis in MCF-7 and HT1080 cells [24]. Our recent study also showed that $MnO_2$ NPs induced hepatic apoptosis of yellow catfish compared to $MnSO_4$ [68]. The aforementioned evidence indicates that an excess of $MnO_2$ NPs triggers inflammatory response and apoptosis, leading to liver injury and hepatotoxicity.

Disruption of hepatic lipid homeostasis is another important factor contributing to

hepatotoxicity, which is mainly manifested in NAFLD [17,18]. NAFLD is a chronic liver disorder observed in vertebrates, characterized by excessive lipid accumulation in hepatocytes [18]. Hepatic lipid accumulation leads to lipotoxicity, a hallmark of NAFLD [17]. Our results show that high dietary $MnO_2$ NPs increased hepatic lipid accumulation and lipogenesis, and decreased lipolysis. To our knowledge, this is the inaugural study on the impact of $MnO_2$ NPs on hepatic lipid metabolism. The diacylglycerol O-acyltransferase 1 (Dgat1) and PPARg play important functions for triglyceride synthesis, and adipose triglyceride lipase (Atgl) is responsible for the hydrolysis of triglycerides [70]. Plin2 is a cytosolic protein predominantly expressed in the liver and associated with the NAFLD development [70]. Importantly, Plin2 coats the lipid droplets membrane and reduces the exposure of adipose triglyceride lipase (Atgl) to lipid droplets, thereby preventing lipolysis [70]. Our study pointed out that high dietary $MnO_2$ NPs significantly upregulated the mRNA and protein expression of Dgat1, Pparg and Plin2, and downregulated *atgl* mRNA levels, further supporting that high dietary $MnO_2$ NPs induce hepatic lipotoxicity through up-regulation of lipogenesis and down-regulation of lipolysis.

The dissection of the mechanism underlying $MnO_2$ NPs-induced hepatic lipotoxicity is crucial for exploiting potential targets in NAFLD treatment. Mitochondrial oxidative stress was considered one of the molecular mechanisms involved in lipotoxicity induced by nanoparticles [17]. Our study indicated that high dietary $MnO_2$ NPs compromise mitochondria function and induce oxidative stress, in agreement with other studies [13,24,31]. Sod2 and CAT are crucial enzymes responsible for mediating antioxidant responses [18,22], and elevated MDA content served as an indicator of cellular damage in animals exposed to nanoparticles [17]. Reduced mitochondrial DNA (mtDNA) copy number and ATP content are biomarkers of oxidative stress [42], which disrupts mitochondrial function and decreases the MMP [22]. Our results show that high $MnO_2$ NPs decrease mtDNA copy number, ATP content Sod2 and Cat activities, and decrease MMP, in agreement with other studies [23,24]. A large flux of mitochondrial-derived $O_2^{\bullet-}$ and mitochondrial dysfunction result in oxidative stress [22]. There is also significant evidence that mtROS induce lipid accumulation [17,22]. Here, Mito-TEMPO pre-incubation abrogated $MnO_2$ NPs-

induced oxidative stress, mitochondrial dysfunction and lipotoxicity, further supporting that mtROS mediated the $MnO_2$ NPs-induced mitochondrial dysfunction and lipotoxicity. Thus, our study reveals that $MnO_2$ NPs increase mitochondrial-derived $O_2^{\cdot-}$ production and cause mitochondrial dysfunction, and accordingly induce hepatic lipid accumulation and lipotoxicity.

Mitochondria are highly dynamic organelles that play a critical role in maintaining cellular functions and are the main target of $MnO_2$ NPs-induced cytotoxicity [23,24]. The balance of mitochondria is maintained by two interconnected processes, mitochondrial dynamics and mitophagy [32]. Several studies have shown that oxidative stress enhances mitochondrial fission, inhibits fusion, and activates mitopahgy [17,32,33]. In our study, high $MnO_2$ NPs increased mitochondrial fission and inhibited mitochondrial fusion. Alterations in mitochondrial dynamics are also involved in the pathogenesis of liver diseases [71]. Palma et al. suggested that the mitochondrial fission pathway is hyperactivated in NAFLD [71]. Therefore, mitochondrial fission and fusion could serve as a quality control mechanism, whereby normal mitochondria are retained through fusion and poor-quality mitochondria are removed through fission. In addition, mitophagy, an evolutionarily conserved process that plays a vital role in preserving cellular homeostasis, offers another quality control mechanism for removing damaged mitochondria [33]. Mitophagy is primarily governed by two molecular pathways: one is the PINK1 (PTEN induced kinase 1)/PRKN (parkin RBR E3 ubiquitin protein ligase)-dependent mitophagy mediated by the ubiquitin proteasome system [33], and another is receptor-mediated mitophagy, involving mitophagy receptors such as Bnip3, Nix, Fundc1, Fkbp8, and Bcl2l13 [34]. Bnip3 is highly expressed in the liver and initiates the process of mitophagy by directly interacting with LC3B [34]. Several studies have indicated that the activation of mitophagy is a protective mechanism to prevent liver injury and attenuate hepatic lipid accumulation [35,36]. Therefore, the activation of mitophagy in our study may act as a protective mechanism to attenuate lipid deposition induced by high $MnO_2$ NPs [17]. Several studies showed that metal- or metal nanoparticles-induced oxidative stress leads to mitochondrial damage and activation of Bnip3-dependent mitophagy [37,38]. Our study indicates that $MnO_2$ NPs

603 significantly upregulate the mRNA and protein expression of *bnip3* and activate
604 mitophagy, and these responses are antagonized by Mito-TEMPO pre-treatment. Thus,
605 our study reveals a novel mechanism whereby $MnO_2$ NPs activate mitophagy through
606 oxidative stress, which may be a protective mechanism against hepatic lipid
607 accumulation and help maintenance of mitochondrial homeostasis.

608 We further explored the mechanism by which $MnO_2$ NPs-induced oxidative stress
609 causes lipid accumulation and mitophagy. Several studies have shown that Hsf1 acts as
610 a sensor of redox homeostasis [22,26,27]. Under oxidative stress, Hsf1 nuclear
611 translocation binds to conserved HSEs to upregulate transcription of HSPs, which serve
612 as molecular chaperones to protect cells from oxidative stress and various diseases [26].
613 Other previous studies also indicated that Hsf1 can regulate lipid metabolism and
614 mitophagy [28,29]. For example, Zhang et al. suggested that the activation of Hsf1 by
615 oxidative stress exacerbated hepatic lipid accumulation [29]. Zhao et al. [72] indicated
616 that Hsf1 regulates mitophagy by binding to HSP60. However, it remains unclear
617 whether Hsf1 directly regulates mitophagy and lipid deposition. Here, we found that
618 the regions of *dgat1*, *plin2* and *bnip3* promoters possess Hsf1 binding sites (HSEs), and
619 that $MnO_2$ NPs significantly enhance the binding activities of Hsf1 to the *dgat1*, *plin2*
620 and *bnip3* promoters. Recently, we reported that Hsf1 targeted *pparg* and mediated the
621 oxidative stress-induced hepatic lipid accumulation after Mn incubation [22],
622 suggesting that Hsf1 linked oxidative stress with $MnO_2$ NPs-induced lipotoxicity. These
623 data indicated that $MnO_2$ NPs promote hepatic lipid accumulation and activate
624 mitophagy by inducing Hsf1. Moreover, we found that Hsf1 knockdown abolished the
625 $MnO_2$ NPs-induced lipotoxicity and mitophagy in hepatocytes, further confirming the
626 central role of Hsf1 in $MnO_2$ NPs-induced lipotoxicity and mitophagy. In addition, a
627 previous study indicated that oxidative stress could induce HSR by promoting Hsf1
628 phosphorylation, thereby enhancing DNA binding activity [26]. Hsf1 phosphorylation
629 occurs under cellular stresses, and its phosphorylation at S326 is vital for transcriptional
630 activation [30]. We show that the increase in $Hsf1^{S326}$ phosphorylation induced by
631 $MnO_2$ NPs can be reversed by Mito-TEMPO pretreatment. However, further studies
632 are needed to elucidate the specific kinase that mediates $Hsf1^{S326}$ phosphorylation

following $MnO_2$ NPs treatment. Taken together, our data reveal that phosphorylation of $Hsf1^{S326}$ acts as a hub between oxidative stress and lipid accumulation as well as mitophagy. Considering that the forms of Mn ($MnO_2$ NPs and $Mn^{2+}$) have differential effects on lipid metabolism in vertebrates [25,48,68], it is necessary to construct different forms of Mn models to explore their differential effects and advantages in future studies.

## 5. Conclusions

In conclusion, we propose a model for the mechanism of $MnO_2$ NPs inducing hepatic lipotoxic disease and mitophagy (Supplementary Fig. 14). Dietary $MnO_2$ NPs induce Mn and lipid accumulation and activate oxidative stress and mitophagy in the liver. The scavenging of mtROS alleviates the $MnO_2$ NPs-induced lipotoxic disease and mitophagy, while mtROS drive the progression of Bnip3-mediated mitophagy. Importantly, we found, for the first time, that $MnO_2$ NPs enhance the Hsf1 binding ability to the *dgat1*, *plin2* and *bnip3* promoters, and accordingly increase lipogenesis and activate mitophagy, respectively. Mechanistically, $MnO_2$ NPs promote lipotoxicity and mitophagy through mtROS-induced phosphorylation of Hsf1 at S326, triggering its nuclear translocation. Our study elucidates the mechanism by which $MnO_2$ NPs induce lipotoxicity and identify Hsf1 as a central regulator of lipid metabolism and mitophagy. Our data highlight the importance of Hsf1 as a potential target of $MnO_2$ NPs- and oxidative stress-associated NAFLD, which provide new insights into the effects of metal oxides nanoparticles on hepatotoxicity in vertebrates.

## Data availability

The data generated in this study are available upon request from the corresponding author.

## Funding statement

This work was supported by the National Key R&D Program of China (2018YFD0900400 to ZL) and Fundamental Research Funds for the Central Universities, China (grant nos. 2662023SCPY001 to Z. L.).

## Declaration of competing interest

The authors declare that there are no conflicts of interest.

**Authorship statement**

ZL and TZ designed the experiments. TZ carried out animal and cell experiments and sample analysis with the help of HZ, JJX, YCX, LLL, XJL and PCX; TZ and ZL analyzed data; TZ drafted the manuscript, and ZL and KP revised the manuscript. All the authors read and approved the manuscript.

**References**

[1] F. Pan, H. Ji, P. Du, T. Huang, C. Wang, W. Liu, Insights into catalytic activation of peroxymonosulfate for carbamazepine degradation by $MnO_2$ nanoparticles in-situ anchored titanate nanotubes: Mechanism, ecotoxicity and DFT study, J. Hazard. Mater. 402 (2021) 123779.

[2] M. Alavi, P. Kamarasu, D.J. McClements, M.D. Moore, Metal and metal oxide-based antiviral nanoparticles: Properties, mechanisms of action, and applications, Adv. Colloid. Interface Sci. 306 (2022) 102726.

[3] O. Maťátková, J. Michailidu, A. Miškovská, I. Kolouchová, J. Masák, A. Čejková, Antimicrobial properties and applications of metal nanoparticles biosynthesized by green methods, Biotechnol. Adv. 58 (2022) 107905.

[4] A. Asaikkutti, P.S. Bhavan, K. Vimala, M. Karthik, P. Cheruparambath, Dietary supplementation of green synthesized manganese-oxide nanoparticles and its effect on growth performance, muscle composition and digestive enzyme activities of the giant freshwater prawn *Macrobrachium rosenbergii*, J. Trace Elem. Med. Biol. 35 (2016) 7-17.

[5] J. Liu, L. Meng, Z. Fei, P.J. Dyson, L. Zhang, On the origin of the synergy between the Pt nanoparticles and $MnO_2$ nanosheets in Wonton-like 3D nanozyme oxidase mimics, Biosens. Bioelectron. 121 (2018) 159-165.

[6] H. Lu, X. Zhang, S.A. Khan, W. Li, L. Wan, Biogenic synthesis of $MnO_2$ nanoparticles with leaf extract of *viola betonicifolia* for enhanced antioxidant, antimicrobial, cytotoxic, and biocompatible applications, Front. Microbiol. 12 (2021) 761084.

[7] N.V. Zaitseva, M.A. Zemlyanova, Toxicologic characteristics of nanodisperse manganese oxide: physical-chemical properties, biological accumulation, and morphological-functional properties at various exposure types, In: J.K. Nduka, M.N. Rashed (Eds.), Heavy Metal Toxicity in Public Health, IntechOpen 2020.

[8] H.F. Krug, P. Wick, Nanotoxicology: an interdisciplinary challenge, Angew. Chem. Int. Ed. Engl. 50 (2011)1260-1278.

[9] R.D. Brohi, L. Wang, H.S. Talpur, D. Wu, F.A. Khan, D. Bhattarai, et al., Toxicity of nanoparticles on the reproductive system in animal models: a review, Front. Pharmacol. 8 (2017) 606.

[10] B.J. Shaw, R.D. Handy, Physiological effects of nanoparticles on fish: a comparison of nanometals versus metal ions, Environ. Int. 37 (2011) 1083-1097.

[11] T. Li, T. Shi, X. Li, S. Zeng, L. Yin, Y. Pu, Effects of Nano-$MnO_2$ on dopaminergic neurons and the spatial learning capability of rats, Int. J. Environ. Res. Public Health 11 (2014) 7918-7930.

[12] X. Chen, G. Wu, Z. Zhang, X. Ma, L. Liu, Neurotoxicity of $Mn_3O_4$ nanoparticles: apoptosis and dopaminergic neurons damage pathway, Ecotoxicol. Environ. Saf. 188 (2020) 109909.

[13] C.Y. Memg, X.Y. Ma, M.Y. Xu, S.F. Pei, Y. Liu, Z.L. Hao, et al., Transcriptomics-based investigation of manganese dioxide nanoparticle toxicity in rats' choroid plexus, Sci. Rep. 13 (2023) 8510.

[14] S.P. Singh, M. Kumari, S.I. Kumari, M.F. Rahman, S.S. Kamal, M. Mahboob, et al., Genotoxicity of nano- and micron-sized manganese oxide in rats after acute oral treatment, Mutat. Res. 754 (2013) 39-50.

[15] C.L. Browning, A. Green, E.P. Gray, R. Hurt, A.B. Kane, Manganese dioxide nanosheets induce mitochondrial toxicity in fish gill epithelial cells, Nanotoxicology 15 (2021) 400-417.

[16] Y. Yao, Y. Zang, J. Qu, M. Tang, T. Zhang, The toxicity of metallic nanoparticles on liver: the subcellular damages, mechanisms, and outcomes, Int. J. Nanomedicine 14 (2019) 8787-8804.

[17] G.H. Chen, C.C. Song, T. Zhao, C. Hogstrand, X.L. Wei, W.H. Lv, Yet al.,

Mitochondria-dependent oxidative stress mediates ZnO nanoparticle (ZnO NP)-induced mitophagy and lipotoxicity in freshwater teleost fish, Environ. Sci. Technol. 56 (2022) 2407-2420.

[18] T. Zhao, K. Wu, C. Hogstrand, Y.H. Xu, G.H. Chen, C.C. Wei, et al., Lipophagy mediated carbohydrate-induced changes of lipid metabolism via oxidative stress, endoplasmic reticulum (ER) stress and ChREBP/PPARγ pathways, Cell. Mol. Life Sci. 77 (2020) 1987-2003.

[19] H. You, X. Wen, X. Wang, C. Zhu, Chen H, Bu L, et al., Derlin-1 ameliorates nonalcoholic hepatic steatosis by promoting ubiquitylation and degradation of FABP1, Free Radic. Biol. Med. 207 (2023) 260-271.

[20] A.A. Hafez, P. Naserzadeh, K. Ashtari, A.M. Mortazavian, A. Salimi, Protection of manganese oxide nanoparticles-induced liver and kidney damage by vitamin D, Regul. Toxicol. Pharmacol. 98 (2018) 240-244.

[21] J. Zhang, Y. Zhao, S. Wang, G. Li, K. Xu, CREBH alleviates mitochondrial oxidative stress through SIRT3 mediating deacetylation of MnSOD and suppression of Nlrp3 inflammasome in NASH, Free Radic. Biol. Med. 190 (2022) 28-41.

[22] T. Zhao, W.H. Lv, C. Hogstrand, D.G. Zhang, Y.C. Xu, Y.H. Xu, et al., Sirt3-Sod2-mROS-mediated manganese triggered hepatic mitochondrial dysfunction and lipotoxicity in a freshwater teleost, Environ. Sci. Technol. 56 (2022) 8020-8033.

[23] S. Alarifi, D. Ali, S. Alkahtani, Oxidative stress-induced DNA damage by manganese dioxide nanoparticles in human neuronal cells, Biomed. Res. Int. 2017 (2017) 5478790.

[24] H.A. Alhadlaq, M.J. Akhtar, M. Ahamed, Different cytotoxic and apoptotic responses of MCF-7 and HT1080 cells to $MnO_2$ nanoparticles are based on similar mode of action, Toxicology 411 (2019) 71-80.

[25] J.J. Xu, B.Y. Jia, T. Zhao, X.Y. Tan, D.G. Zhang, C.C. Song, et al., Influences of five dietary manganese sources on growth, feed utilization, lipid metabolism, antioxidant capacity, inflammatory response and endoplasmic reticulum stress in yellow catfish intestine, Aquaculture 566 (2023) 739190.

[26] J. Barna, P. Csermely, T. Vellai, Roles of heat shock factor 1 beyond the heat shock

response, Cell. Mol. Life Sci. 75 (2018) 2897-2916.

[27] R. Gomez-Pastor, E.T. Burchfiel, D.J. Thiele, Regulation of heat shock transcription factors and their roles in physiology and disease, Nat. Rev. Mol. Cell Biol. 19 (2018) 4-19.

[28] M. Li, J. Hu, R. Jin, H. Cheng, H. Chen, L. Li, et al., Effects of LRP1B regulated by HSF1 on lipid metabolism in hepatocellular carcinoma, J. Hepatocell. Carcinoma 7 (2020) 361-376.

[29] D.G. Zhang, X.J. Xu, K. Pantopoulos, T. Zhao, H. Zheng, Z. Luo, HSF1-SELENOS pathway mediated dietary inorganic Se-induced lipogenesis via the up-regulation of PPARγ expression in yellow catfish, Biochim. Biophys. Acta Gene Regul. Mech. 1865 (2022) 194802.

[30] B. Zhang, Y. Fan, P. Cao, K. Tan, Multifaceted roles of HSF1 in cell death: A state-of-the-art review, Biochim. Biophys. Acta Rev. Cancer 1876 (2021) 188591.

[31] A.A. Hafez, P. Naserzadeh, A.M. Mortazavian, B. Mehravi, K. Ashtari, E. Seydi, et al., Comparison of the effects of $MnO_2$-NPs and $MnO_2$-MPs on mitochondrial complexes in different organs, Toxicol. Mech. Methods 29 (2019) 86-94.

[32] Y. Jiang, S. Krantz, X. Qin, S. Li, H. Gunasekara, Y.M. Kim, et al., Caveolin-1 controls mitochondrial damage and ROS production by regulating fission - fusion dynamics and mitophagy, Redox Biol. 52 (2022) 102304.

[33] S. Pickles, P. Vigié, R.J. Youle, Mitophagy and quality control mechanisms in mitochondrial maintenance, Curr. Biol. 28 (2018) R170-R185.

[34] P. Terešak, A. Lapao, N. Subic, P. Boya, Z. Elazar, A. Simonsen, Regulation of PRKN-independent mitophagy, Autophagy 18 (2022) 24-39.

[35] D. Glick, W. Zhang, M. Beaton, G. Marsboom, M. Gruber, M.C. Simon, et al., BNip3 regulates mitochondrial function and lipid metabolism in the liver, Mol. Cell. Biol. 32 (2012) 2570-2584.

[36] C. Shi, Z. Zhang, R. Xu, Y. Zhang, Z. Wang, Contribution of HIF-1α/BNIP3-mediated autophagy to lipid accumulation during irinotecan-induced liver injury, Sci. Rep. 13 (2023) 6528.

[37] H.L. Zhu, X.T. Shi, X.F. Xu, G.X. Zhou, Y.W. Xiong, S.J. Yi, et al., Melatonin

protects against environmental stress-induced fetal growth restriction via suppressing ROS-mediated GCN2/ATF4/BNIP3-dependent mitophagy in placental trophoblasts, Redox Biol. 40 (2021) 101854.

[38] J. Liu, Z. Huang, S. Yin, X. Zhou, Y. Jiang, L. Shao, The lysosome-mitochondrion crosstalk engaged in silver nanoparticles-disturbed mitochondrial homeostasis, Sci. Total. Environ. 889 (2023) 164078.

[39] G.S. Hotamisligil, Inflammation and metabolic disorders, Nature 444 (2006) 860-867.

[40] G. Gong, C. Dan, S. Xiao, W. Guo, P. Huang, Y. Xiong, et al., Chromosomal-level assembly of yellow catfish genome using third-generation DNA sequencing and Hi-C analysis, Gigascience 7 (2018) giy120.

[41] Y.F. Song, C. Hogstrand, S.C. Ling, G.H. Chen, Z. Luo, Creb-Pgc1α pathway modulates the interaction between lipid droplets and mitochondria and influences high fat diet-induced changes of lipid metabolism in the liver and isolated hepatocytes of yellow catfish, J. Nutr. Biochem. 80 (2020) 108364.

[42] D.G. Zhang, W.S. Kunz, X.J. Lei, E. Zito, T. Zhao, Y.C. Xu, et al., Selenium ameliorated oxidized fish oil-induced lipotoxicity via the inhibition of mitochondrial oxidative stress, remodeling of Usp4-mediated deubiquitination and stabilization of Pparα, Antioxid. Redox Signal. (2023). Ahead of print. https://doi.org/10.1089/ars.2022.0194

[43] G.H. Chen, C.C. Song, K. Pantopoulos, X.L. Wei, H. Zheng, Z. Luo, Mitochondrial oxidative stress mediated Fe-induced ferroptosis via the NRF2-ARE pathway, Free Radic. Biol. Med. 180 (2022) 95-107.

[44] L.X. Wu, Y.C. Xu, K. Pantopoulos, X.Y. Tan, X.L. Wei, H. Zheng, et al., Glycophagy mediated glucose-induced changes of hepatic glycogen metabolism via OGT1-AKT1-FOXO1Ser238 pathway, J. Nutr. Biochem. 117 (2023) 109337.

[45] M.C. Mancini, R.C. Noland, J.J. Collier, S.J. Burke, K. Stadler, T.D. Heden, Lysosomal glucose sensing and glycophagy in metabolism, Trends Endocrinol. Metab. 34 (2023) 764-777.

[46] Y.M. Wang, H. Tang, Y.J. Tang, J. Liu, Y.F. Yin, Y.L. Tang, et al., ASIC1/RIP1

accelerates atherosclerosis via disrupting lipophagy, J. Adv. Res. (2023). https://doi.org/10.1016/j.jare.2023.11.004.

[47] T. Cedervall, L.A. Hansson, M. Lard, B. Frohm, S. Linse, Food chain transport of nanoparticles affects behaviour and fat metabolism in fish, PLoS One 7 (2012) e32254.

[48] T. Zhao, X.Y. Tan, K. Pantopoulos, J.J. Xu, H. Zheng, Y.C. Xu, et al, miR-20a-5p targeting *mfn2*-mediated mitochondria-lipid droplet contacts regulated differential changes in hepatic lipid metabolism induced by two Mn sources in yellow catfish, J. Hazard. Mater. 462 (2024) 132749.

[49] J.J. Xu, T. Zhao, Z. Luo, C.C. Zhong, H. Zheng, X.Y. Tan, Effects of dietary supplementation with manganese dioxide nanoparticles on growth, Mn metabolism and kidney health of yellow catfish *Pelteobagrus fulvidraco*, Aquacult. Rep. 33 (2023) 101815.

[50] T.C. Leuthner, J.H. Hartman, I.T. Ryde, J.N. Meyer, PCR-based determination of mitochondrial DNA copy number in multiple species, Methods Mol. Biol. 2310 (2021) 91-111.

[51] H. Guo, T. Fang, Y. Cheng, T. Li, J.R. Qu, C.F. Xu, et al., ChREBP-β/TXNIP aggravates frucose-induced renal injury through triggering ferroptosis of renal tubular epithelial cells, Free Radic. Biol. Med. 199 (2023) 154-165.

[52] S. Dayalan Naidu, C. Sutherland, Y. Zhang, A. Risco, L. de la Vega, C.J. Caunt, et al., Heat shock factor 1 is a substrate for p38 mitogen-activated protein kinases, Mol. Cell. Biol. 36 (2016) 2403-2417.

[53] D.C. Chan, Mitochondrial dynamics and its involvement in disease, Annu. Rev. Pathol. 15 (2020) 235-259.

[54] Z. Tang, S. Dai, Y. He, R.A. Doty, L.D. Shultz, S.B. Sampson, et al., MEK guards proteome stability and inhibits tumor-suppressive amyloidogenesis via HSF1, Cell 160 (2015) 729-744.

[55] K.H. Su, J. Cao, Z. Tang, S. Dai, Y. He, S.B. Sampson, et al., HSF1 critically attunes proteotoxic stress sensing by mTORC1 to combat stress and promote growth, Nat. Cell Biol. 18 (2016) 527-539.

[56] W.C. Lu, R. Omari, H. Ray, J. Wang, I. Williams, C. Jacobs, et al., AKT1 mediates multiple phosphorylation events that functionally promote HSF1 activation, FEBS J. 289 (2022) 3876-3893.

[57] J.L. Aschner, M. Aschner, Nutritional aspects of manganese homeostasis, Mol. Aspects Med. 26 (2005) 353-362.

[58] K.J. Horning, S.W. Caito, K.G. Tipps, A.B. Bowman, M. Aschner, Manganese is essential for neuronal health, Annu. Rev. Nutr. 35 (2015) 71-108.

[59] W. Lin, D.R. Vann, P.T. Doulias, T. Wang, G. Landesberg, X. Li, et al., Hepatic metal ion transporter ZIP8 regulates manganese homeostasis and manganese-dependent enzyme activity, J. Clin. Invest. 127 (2017) 2407-2417.

[60] C.K. Fung, N. Zhao, The combined inactivation of intestinal and hepatic ZIP14 exacerbates manganese overload in mice, Int. J. Mol. Sci. 23 (2022) 6495.

[61] A.V. Menon, J. Chang, J. Kim, Mechanisms of divalent metal toxicity in affective disorders, Toxicology 339 (2016) 58-72.

[62] M.S. Madejczyk, N. Ballatori, The iron transporter ferroportin can also function as a manganese exporter, Biochim. Biophys. Acta 1818 (2012) 651-657.

[63] E.K. Choi, T.T. Nguyen, N. Gupta, S. Iwase, Y.A. Seo, Functional analysis of *SLC39A8* mutations and their implications for manganese deficiency and mitochondrial disorders, Sci. Rep. 8 (2018) 3163.

[64] K.J. Thompson, M. Wessling-Resnick, ZIP14 is degraded in response to manganese exposure, Biometals 32 (2019) 829-843.

[65] F. Zhao, Y. Zhao, Y. Liu, X. Chang, C. Chen, Y. Zhao, Cellular uptake, intracellular trafficking, and cytotoxicity of nanomaterials, Small 7 (2011) 1322-1337.

[66] V. Vilas-Boas, M. Vinken, Hepatotoxicity induced by nanomaterials: mechanisms and in vitro models, Arch. Toxicol. 95 (2021) 27-52.

[67] S. Mohammed, E.H. Nicklas, N. Thadathil, R. Selvarani, G.H. Royce, M. Kinter, et al., Role of necroptosis in chronic hepatic inflammation and fibrosis in a mouse model of increased oxidative stress, Free Radic. Biol. Med. 164 (2021) 315-328.

[68] T. Zhao, H. Zheng, J.J. Xu, L.L. Liu, K. Z. Luo, $MnO_2$ nanoparticles and $MnSO_4$ differentially affected hepatic lipid metabolism through miR-92a/*acsl3*-dependent

*de novo* lipogenesis in yellow catfish *Pelteobagrus fulvidraco*. Environ. Pollut. 336 (2023) 122416.

[69] K. Ding, X. Li, X. Ren, N. Ding, L. Tao, X. Dong, et al., GBP5 promotes liver injury and inflammation by inducing hepatocyte apoptosis, FASEB J. 36 (2022) e22119.

[70] E. Scorletti, R.M. Carr, A new perspective on NAFLD: Focusing on lipid droplets, J. Hepatol. 76 (2022) 934-945.

[71] E. Palma, A. Riva, C. Moreno, G. Odena, S. Mudan, N. Manyakin, et al., Perturbations in mitochondrial dynamics are closely involved in the progression of alcoholic liver disease, Alcohol Clin. Exp. Res. 44 (2020) 856-865.

[72] Y. Zhao, H.X. Li, Y. Luo, J.G. Cui, M. Talukder, J.L. Li, Lycopene mitigates DEHP-induced hepatic mitochondrial quality control disorder via regulating SIRT1/PINK1/mitophagy axis and mitochondrial unfolded protein response, Environ. Pollut. 292(Pt B) (2022) 118390.

903

904

905

906 **Figure captions**

907 **Fig. 1. Dose-dependent effects of dietary $MnO_2$ NPs on the hepatic lipid content in**
908 **yellow catfish.** (A) Representative images of liver; scale bars, 1 cm, **(**B and C)
909 Representative microphotograph of liver tissues stained by H&E (B) and Oil-red O (C).
910 200× magnification; scale bars, 50 μm, respectively. (D) TGs content; (E and F)
911 Relative areas for hepatic vacuoles after H&E staining and lipid droplets after Oil Red
912 O staining, respectively. Lipids appear red, and nuclei appear blue after Oil Red O
913 staining. The depth of red color and the size of lipid droplets were positively correlated
914 with lipid content. Va, vacuoles; Ld, lipid droplets. Values are means ± S.E.M. [For
915 analyzing hepatic TGs content, n= 3 represents three replicate tanks for each treatment
916 and was used as three biological replicates. At least 6 fish were sampled for each tank
917 and used as technical replicates); For analyzing H&E and ORO relative areas, n= 3
918 represents three replicate tanks for each treatment and was used as three biological
919 replicates. At least 3 fish were sampled for each tank and used as technical replicates].
920 *P* value was calculated by one-way ANOVA and further post hoc Duncan's multiple
921 range testing. Values without the same letter indicate significant difference among three
922 treatments ($P < 0.05$).

923 **Fig. 2. Dose-dependent effects of dietary MnO2 NPs on hepatic mitochondrial**
924 **function and Hsf1 expression and localization in yellow catfish.** (A) RT-PCR for
925 mtDNA copy number; (B) Relative quantification of mtDNA copy number; (C) ATP

content; (D) Sod2 activity; (E) Cat activity; (F) MDA content; (G) The ratio of GSH/GSSG; (H) mRNA expression of antioxidant and heat shock proteins related genes; (I) Western blot analysis of p-Hsf1$^{S326}$, Hsf1 and N-Hsf1; (J) Relative quantification of p-Hsf1$^{S326}$, Hsf1 and N-Hsf1 protein levels; (K) Immunofluorescence images of Hsf1; Scale bars: 10 μm; The white arrows represent the co-localization of Hsf1 with the nucleus; (L) Relative fluorescence intensity of Hsf1. Relative mRNA expression values were normalized to housekeeping genes (*ubce* and *rpl7*) expressed as a ratio of the control. Values are means ± S.E.M. (n= 3). *P* value was calculated by one-way ANOVA and post hoc Duncan's multiple range testing. Values without the same letter indicate significant difference among three treatments ($P < 0.05$).

**Fig. 3. Effects of dietary $MnO_2$ NPs levels on hepatic mitophagy in yellow catfish.** (A) Representative ultrastructural images of liver tissue; Ld, lipid droplet; M, mitochondria; N, nucleus; AV, autophagosome vacuoles; The yellow dotted line represents mitophagy; (B) mRNA expression of mitophagy and autophagy -related genes; (C) Western blot analysis of autophagy and mitophagy-related proteins; (D) Relative quantification of autophagy and mitophagy-related proteins; (E) Relative quantification of of Lc3b and Bnip3 proteins on mitochondria. Relative mRNA expression values were normalized to housekeeping genes (*ubce* and *rpl7*) expressed as a ratio of the control. Values are means ± S.E.M. n= 3. *P* value was calculated by one-way ANOVA and post hoc Duncan's multiple range testing. Values without the same letter indicate significant difference among three treatments ($P < 0.05$).

**Fig. 4. $MnO_2$ NPs incubation activates mitophagy in hepatocytes of yellow catfish.**

The primary hepatocytes from yellow catfish were incubated in control or $MnO_2$ NPs for 48h in M199 medium. (A) mRNA expression of mitophagy and autophagy -related genes; (B) Western blot analysis of autophagy and mitophagy-related proteins; (C) Relative quantification of autophagy and mitophagy-related proteins; (D) Representative ultrastructural images of hepatocytes; Ld, lipid droplet; N, nucleus; Black arrows represent the mitochondria, red arrows represent the mitophagy, yellow arrows represent nanoparticle endocytosis, blue arrows represent nanoparticles; (E) Immunofluorescence images of Lc3b and Bnip3; Scale bars: 10 μm; White arrows represent the colocalization of the two proteins; (F) Immunofluorescence images of Lc3b and Tom20; Scale bars: 10 μm. Relative mRNA expression values were normalized to housekeeping genes (*elfa* and *rpl7*) expressed as a ratio of the control. Values are means ± S.E.M. n = 3. *P* value was calculated by one-way ANOVA and post hoc Duncan's multiple range testing. Values without the same letter indicate significant difference among three treatments ($P < 0.05$).

**Fig. 5. Hsf1 mediates $MnO_2$ NPs-induced mitophagy in hepatocytes of yellow catfish.** The primary hepatocytes were incubated in control or $MnO_2$ NPs in M199 medium with or without treatment with *hsf1* knockdown for 48 h. (A) mRNA expression of mitophagy and autophagy -related genes; (B) Western blot analysis of autophagy and mitophagy-related proteins; (C) Relative quantification of autophagy and mitophagy-related proteins; (D) Immunofluorescence images of Lc3b and Bnip3; Scale bars: 10 μm; White arrows represent the colocalization of the two proteins; (E) Relative quantification of Lc3b and Bnip3 colocalization. Relative mRNA expression

values were normalized to housekeeping genes (β-*actin* and *elfa*) expressed as a ratio of the si-NC. Values are means ± S.E.M. n = at least 3. *P* value was calculated by Student's *t* tests. $^{*}P < 0.05$, $^{**}P < 0.01$, compared with si-NC; $^{\#}P < 0.05$, $^{\#\#}P < 0.01$, compared with $MnO_2$ NPs + si-NC group.

**Fig. 6. $MnO_2$ NPs transcriptionally activate Bnip3 expression by promoting the binding of Hsf1 to the *bnip3* promoter.** (A) Hsf1 binding sequence (HSE) located at -922 bp to -893 bp of *bnip3* promoter of yellow catfish; (B) Site-mutation analysis of Hsf1 binding sites on pGl3-*bnip3*-1675/+60 vectors in HEK 293T cells treated with 20 μg/ml $MnO_2$ NPs for 48h; (C) The yellow catfish *hsf1* gene was overexpressed in HEK293T cells for 48 h; (D) Site-mutation analysis of Hsf1 binding sites on pGl3-*bnip3*-1675/+60 vectors in HEK 293T cells treated with pcDNA3.1-HA-Hsf1 overexpression for 48h. (E) EMSA of putative Hsf1 binding sequences (HSE). The 5′-biotin labeled double-stranded oligomers were incubated with nuclear protein in yellow catfish hepatocytes. A 200-fold excess of the competitor and mutative competitor oligomers were added to the competition and mutant competition assay, respectively. (F and G) ChIP assay for *bnip3* promoter binding with Hsf1 by agarose gel electrophoresis and qRT-PCR in hepatocytes. Values are means ± SEM (n = 3). *P* value was calculated by Student's *t* tests. $^{*}P < 0.05$, $^{**}P < 0.01$, compared with the control; $^{\#}P < 0.05$, $^{\#\#}P < 0.01$ compared with relative luciferase activity between two promoters.

**Fig. 7. Hsf1 mediates $MnO_2$ NPs-induced lipogenesis and lipid accumulation in hepatocytes of yellow catfish.** The yellow catfish hepatocytes incubated in control or $MnO_2$ NPs in M199 medium with or without treatment with *hsf1* knockdown for 48 h.

(A) TGs content; (B) The presence of Bodipy 493/503–stained lipid droplet was demonstrated by flow cytometry; (C) The lipid content quantified by flow cytometric analysis of FL1 (green) mean fluorescence intensity after Bodipy 493/503 staining; (D) Representative confocal microscopy image of yellow catfish hepatocytes after 5μg/ml BODIPY 493/503 staining. Scale bars, 25 μm. (E) mRNA expression of *dgat1* and *plin2*. (F and G) Protein levels of Dgat1 and Plin2. Relative mRNA expression values were normalized to housekeeping genes (β-*actin* and *elfa*) expressed as a ratio of the si-NC. Values are means ± S.E.M. (n = 3). *P* value was calculated by Student's *t* tests. $^{*}P < 0.05$, $^{**}P < 0.01$, compared with si-NC; $^{\#}P < 0.05$, $^{\#\#}P < 0.01$, compared with $MnO_2$ NPs + si-NC group.

**Fig. 8. $MnO_2$ NPs transcriptionally induce *plin2* and *dgat1* expression by promoting the binding of Hsf1 to the *plin2* and *dgat1* promoters.** (A and B) Hsf1 binding sequence (HSE) located at -755 bp to -725 bp of *plin3* promoter region and -868 bp to -838 bp of *dgat1* promoter region of yellow catfish; (C and D) Site-mutation analysis of Hsf1 binding sites on pGl3-*plin2*-822/+33 and pGl3-*dgat1*-1489/+42 vectors in HEK 293T cells treated with 20 μg/ml $MnO_2$ NPs for 48h; (E and F) Site-mutation analysis of Hsf1 binding sites on pGl3-*plin2*-822/+33 and pGl3-*dgat1*-1489/+42 vectors in HEK 293T cells treated with pcDNA3.1-HA-Hsf1 overexpression for 48h. (G and H) EMSA of putative Hsf1 binding sequences (HSE). The 5′-biotin labeled double-stranded oligomers were incubated with nuclear protein in yellow catfish hepatocytes. A 200-fold excess of the competitor and mutative competitor oligomers were added to the competition and mutant competition assay, respectively.

(I-K) ChIP assay for *plin2* and *dgat1* promoters binding with Hsf1 by agarose gel electrophoresis and qPCR in hepatocytes. Values are means ± SEM (n = 3). *P* value was calculated by Student's *t* tests. $^{*}P < 0.05$, $^{**}P < 0.01$, compared with the Control; $^{\#\#}P < 0.01$ compared with relative luciferase activity between two promoter regions.

**Figure 1**

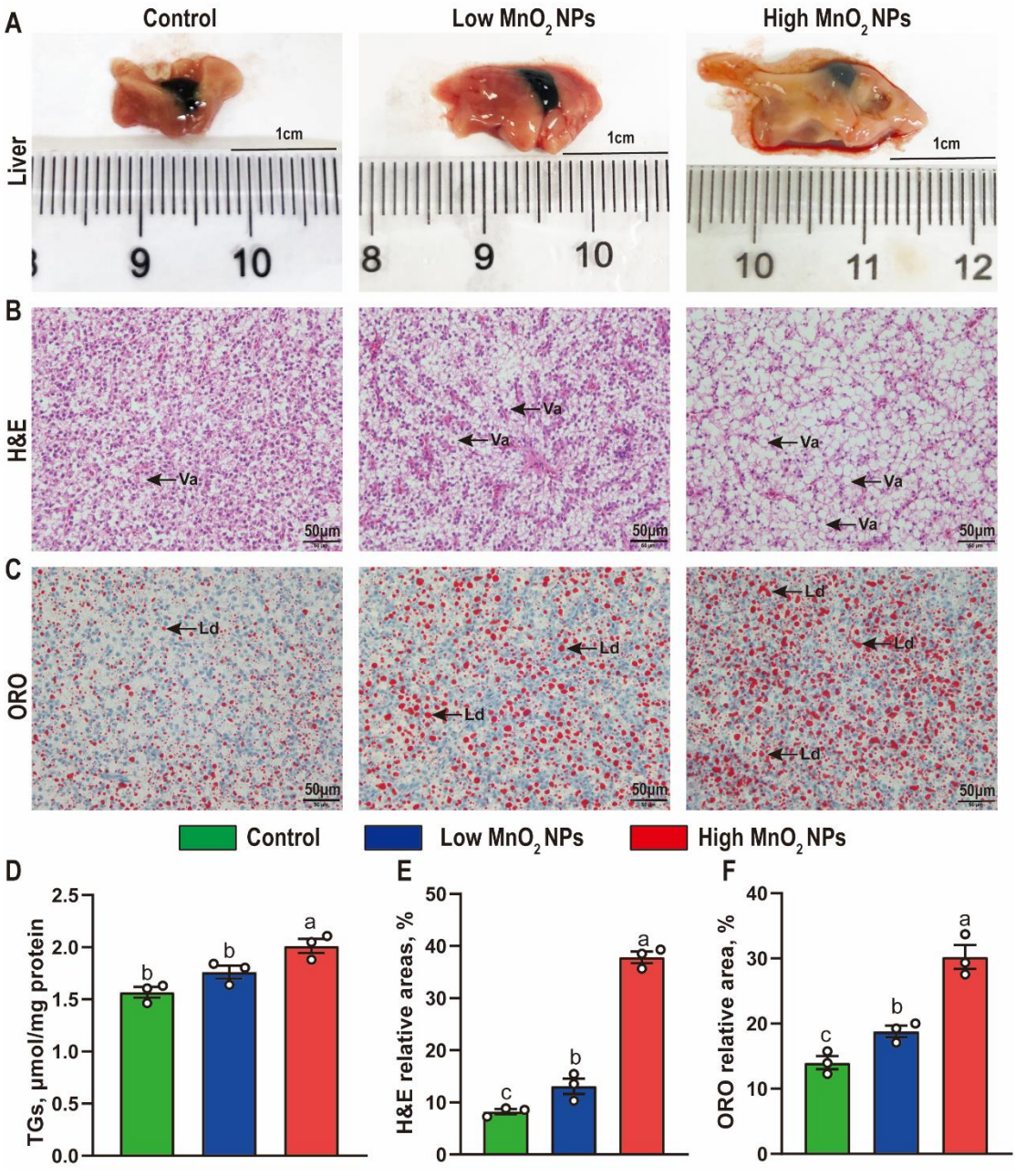
A
Control
Low MnO2 NPs
High MnO2 NPs
Liver
1cm
B
H&E
Va
50μm
C
ORO
Ld
Control
Low MnO2 NPs
High MnO2 NPs
D
TGs, μmol/mg protein
E
H&E relative areas, %
F
ORO relative area, %
a
b
c

**Figure 2**

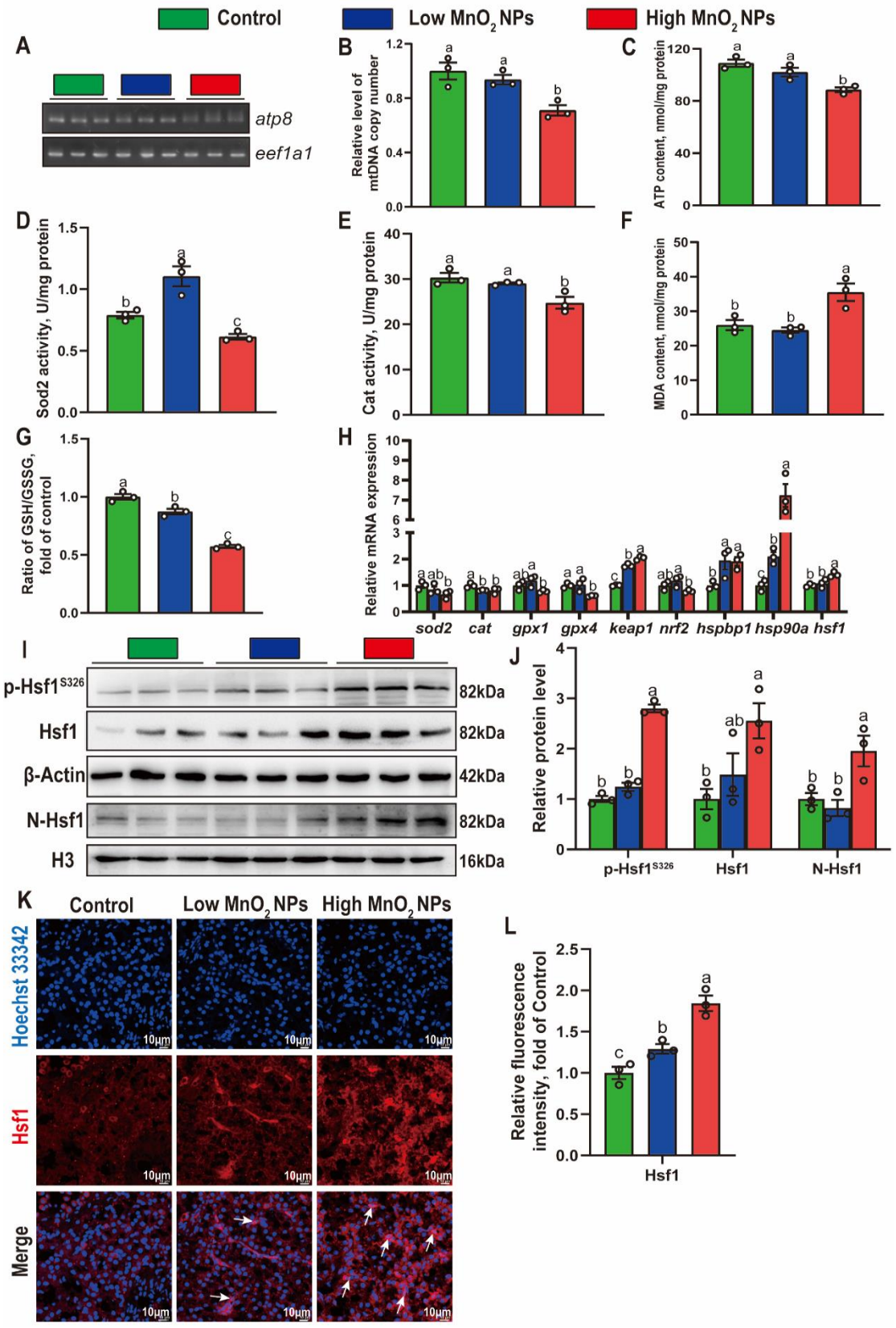
Control
Low MnO2 NPs
High MnO2 NPs
A
atp8
eef1a1
B
Relative level of mtDNA copy number
C
ATP content, nmol/mg protein
D
Sod2 activity, U/mg protein
E
Cat activity, U/mg protein
F
MDA content, nmol/mg protein
G
Ratio of GSH/GSSG, fold of control
H
Relative mRNA expression
sod2
cat
gpx1
gpx4
keap1
nrf2
hspbp1
hsp90a
hsf1
I
p-Hsf1S326
Hsf1
β-Actin
N-Hsf1
H3
82kDa
82kDa
42kDa
82kDa
16kDa
J
Relative protein level
p-Hsf1S326
Hsf1
N-Hsf1
K
Control
Low MnO2 NPs
High MnO2 NPs
Hoechst 33342
Hsf1
Merge
10μm
L
Relative fluorescence intensity, fold of Control
Hsf1

**Figure 3**

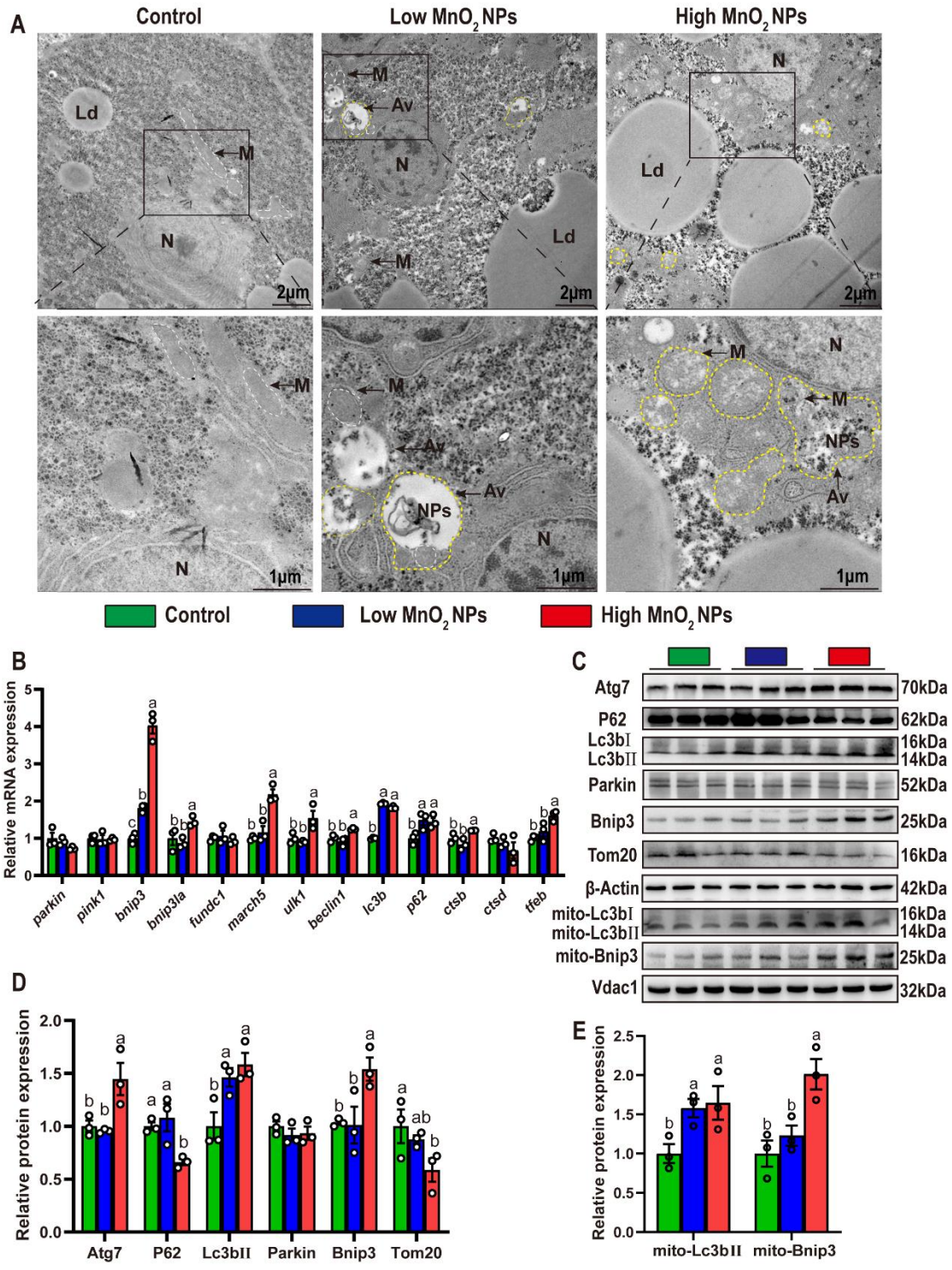
A
Control
Low MnO2 NPs
High MnO2 NPs
Ld
M
N
Av
NPs
2μm
1μm
Control
Low MnO2 NPs
High MnO2 NPs
B
Relative mRNA expression
parkin
pink1
bnip3
bnip3la
fundc1
march5
ulk1
beclin1
lc3b
p62
ctsb
ctsd
tfeb
C
Atg7
P62
Lc3bⅠ
Lc3bⅡ
Parkin
Bnip3
Tom20
β-Actin
mito-Lc3bⅠ
mito-Lc3bⅡ
mito-Bnip3
Vdac1
70kDa
62kDa
16kDa
14kDa
52kDa
25kDa
16kDa
42kDa
16kDa
14kDa
25kDa
32kDa
D
Relative protein expression
Atg7
P62
Lc3bII
Parkin
Bnip3
Tom20
E
Relative protein expression
mito-Lc3bII
mito-Bnip3

**Figure 4**

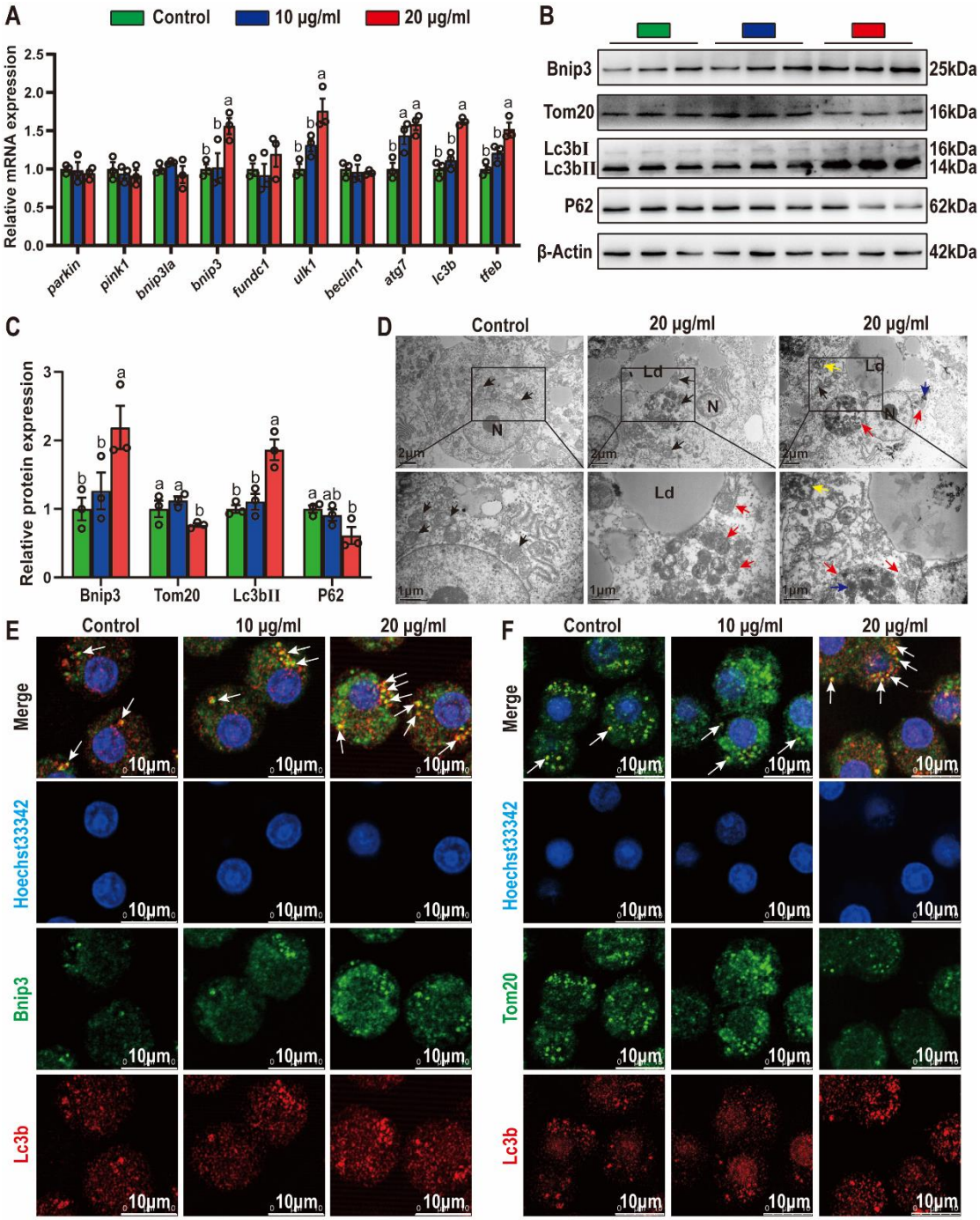


**Figure 5**

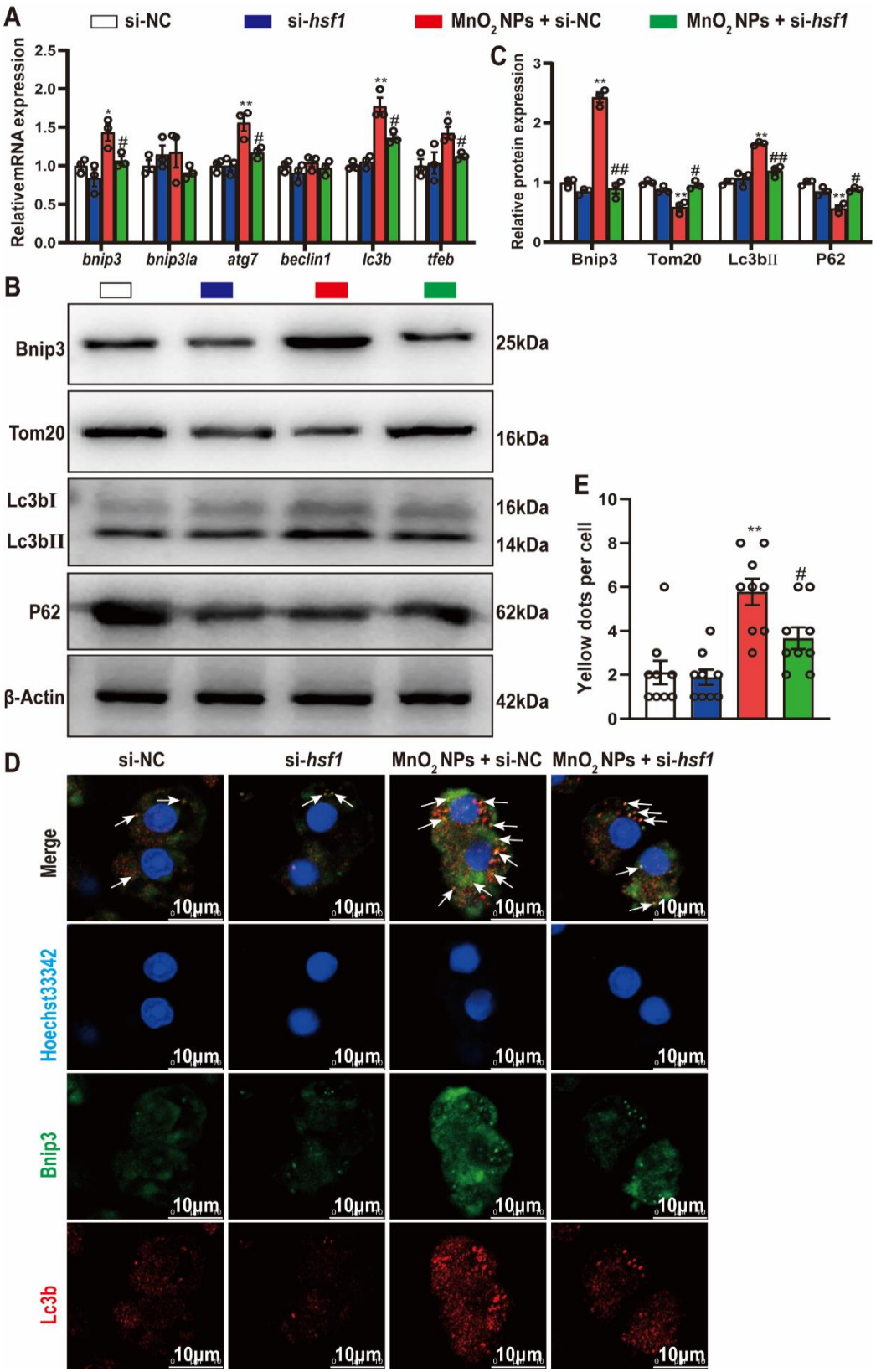
A
si-NC
si-hsf1
MnO2 NPs + si-NC
MnO2 NPs + si-hsf1
Relative mRNA expression
bnip3
bnip3la
atg7
beclin1
lc3b
tfeb
C
Relative protein expression
Bnip3
Tom20
Lc3bII
P62
B
Bnip3
Tom20
Lc3bI
Lc3bII
P62
β-Actin
25kDa
16kDa
16kDa
14kDa
62kDa
42kDa
E
Yellow dots per cell
D
si-NC
si-hsf1
MnO2 NPs + si-NC
MnO2 NPs + si-hsf1
Merge
Hoechst33342
Bnip3
Lc3b
10μm

**Figure 6**

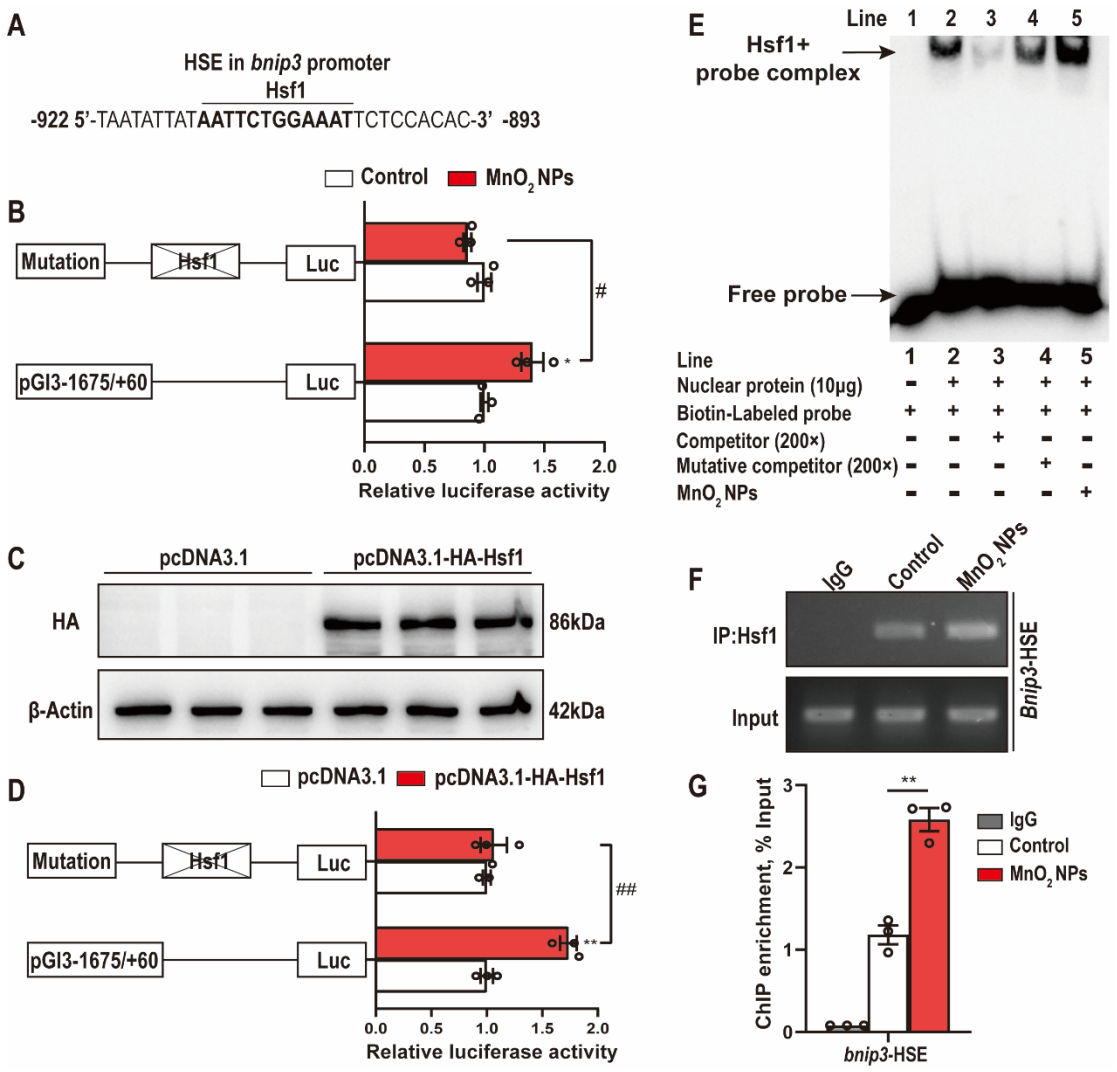
A
HSE in bnip3 promoter
Hsf1
-922 5'-TAATATTATAATTCTGGAAATTCTCCACAC-3' -893
B
Control
MnO2 NPs
Mutation
Hsf1
Luc
pGl3-1675/+60
Luc
#
*
0.0 0.5 1.0 1.5 2.0
Relative luciferase activity
C
pcDNA3.1
pcDNA3.1-HA-Hsf1
HA
86kDa
β-Actin
42kDa
D
pcDNA3.1
pcDNA3.1-HA-Hsf1
Mutation
Hsf1
Luc
pGl3-1675/+60
Luc
##
**
0.0 0.5 1.0 1.5 2.0
Relative luciferase activity
E
Line 1 2 3 4 5
Hsf1+
probe complex
Free probe
Line 1 2 3 4 5
Nuclear protein (10μg) - + + + +
Biotin-Labeled probe + + + + +
Competitor (200×) - - + - -
Mutative competitor (200×) - - - + -
MnO2 NPs - - - - +
F
IgG
Control
MnO2 NPs
IP:Hsf1
Input
Bnip3-HSE
G
**
ChIP enrichment, % Input
0 1 2 3
IgG
Control
MnO2 NPs
bnip3-HSE

**Figure 7**

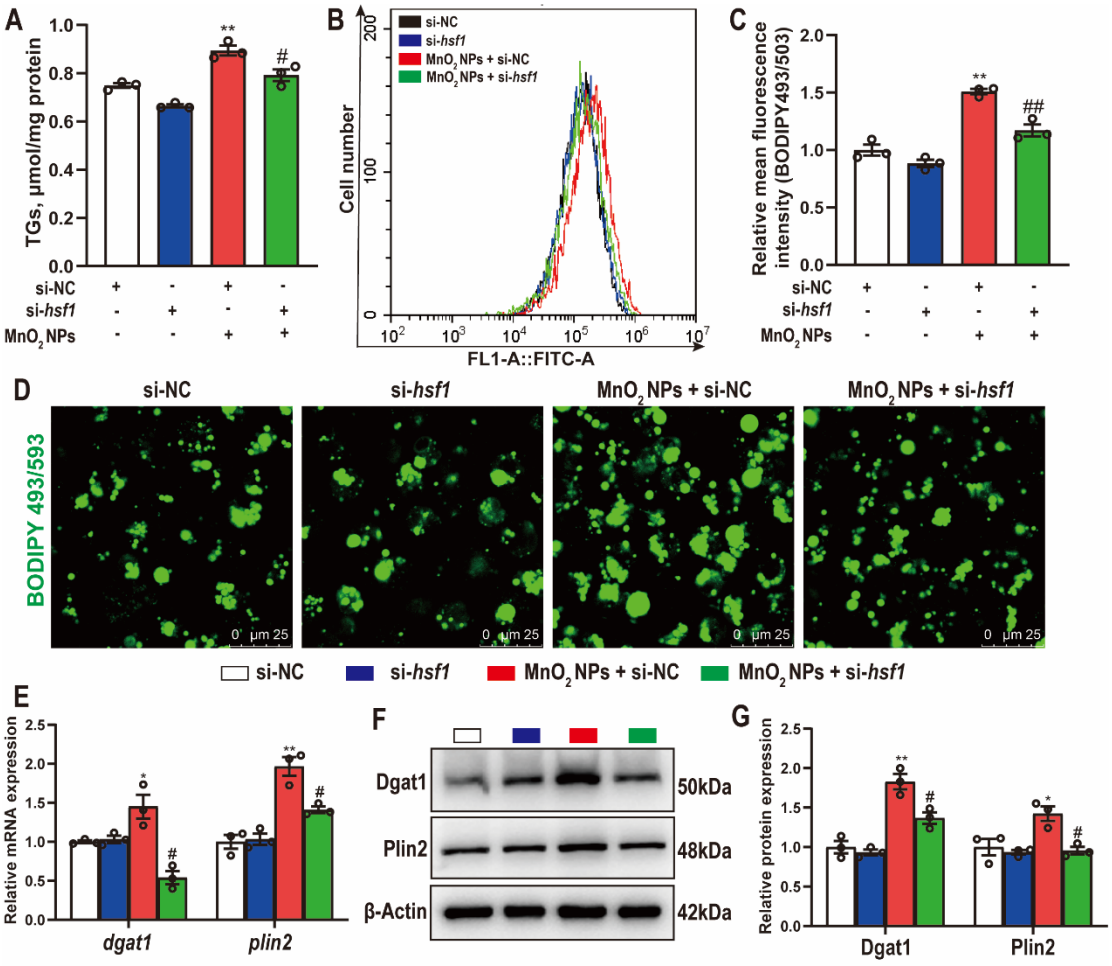
A
TGs, μmol/mg protein
si-NC
si-hsf1
MnO2 NPs
B
Cell number
FL1-A::FITC-A
si-NC
si-hsf1
MnO2 NPs + si-NC
MnO2 NPs + si-hsf1
C
Relative mean fluorescence intensity (BODIPY493/503)
D
BODIPY 493/593
E
Relative mRNA expression
dgat1
plin2
F
Dgat1
Plin2
β-Actin
50kDa
48kDa
42kDa
G
Relative protein expression

**Figure 8**

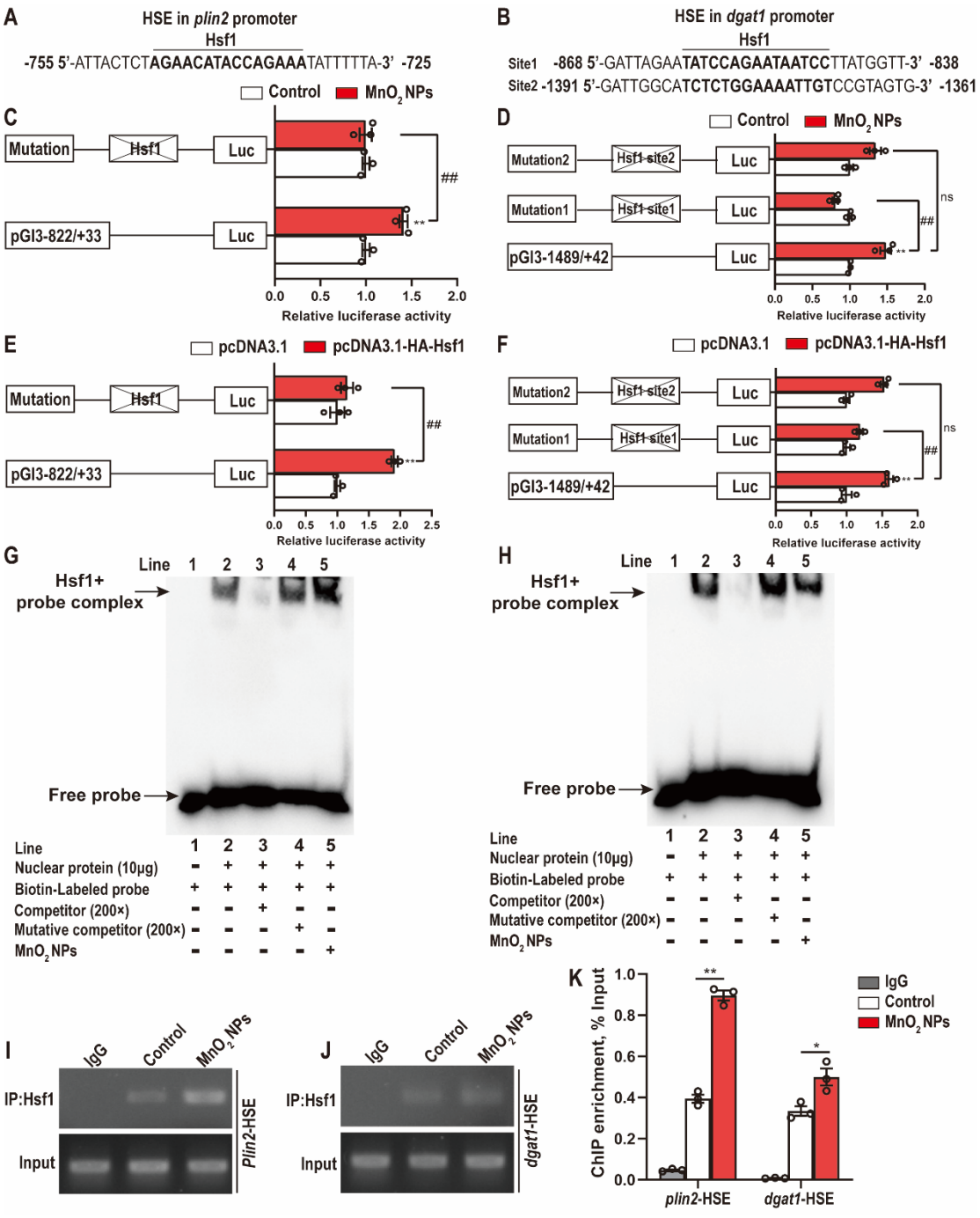
A
HSE in plin2 promoter
Hsf1
-755 5'-ATTACTCTAGAACATACCAGAAATATTTTTA-3' -725
B
HSE in dgat1 promoter
Hsf1
Site1 -868 5'-GATTAGAATATCCAGAATAATCCTTATGGTT-3' -838
Site2 -1391 5'-GATTGGCATCTCTGGAAAATTGTCCGTAGTG-3' -1361
Control
MnO2 NPs
C
Mutation
Hsf1
Luc
pGl3-822/+33
Relative luciferase activity
D
Mutation2
Hsf1-site2
Mutation1
Hsf1-site1
pGl3-1489/+42
ns
E
pcDNA3.1
pcDNA3.1-HA-Hsf1
F
G
Line 1 2 3 4 5
Hsf1+
probe complex
Free probe
Line 1 2 3 4 5
Nuclear protein (10μg) - + + + +
Biotin-Labeled probe + + + + +
Competitor (200×) - - + - -
Mutative competitor (200×) - - - + -
MnO2 NPs - - - - +
H
Mutative competitor (200×) - - - + -
I
IgG
Control
MnO2 NPs
IP:Hsf1
Input
Plin2-HSE
J
dgat1-HSE
K
ChIP enrichment, % Input
plin2-HSE
dgat1-HSE